THE BIOPHYSICAL BASIS UNDERLYING THE MAINTENANCE OF EARLY PHASE LONG-TERM POTENTIATION

Abbreviated title: AMPAR trafficking during early phase LTP

Moritz F. P. Becker [*,1] and Christian Tetzlaff[1,2]

[1]III. Institute of Physics – Biophysics, Georg-August University, 37077 Göttingen, Germany
[2]Bernstein Center for Computational Neuroscience, 37075 Göttingen, Germany

*Correspondence to:
Moritz Becker
Department for Computational Neuroscience, III. Institute of Physics - Biophysics
University of Göttingen
Friedrich-Hund-Platz 1
37077 Göttingen
Germany
moritz.becker@phys.uni-goettingen.de

Pages: 53
Figures: 10
Tables: 4
Abstract length: 163/250
Introduction length: 668/650
Discussion length: 1413/1500
Significance statement length: 120/120

Conflict of Interest Statement: The authors declare no competing financial interests.

Acknowledgments: We would like to thank Silvio Rizzoli for many fruitful discussions and various helpful comments on this study. The research was funded by the German Research Foundation (CRC1286, project C1 and project #419866478).

Abstract

The maintenance of synaptic changes resulting from long-term potentiation (LTP) is essential for brain functions. Different LTP phases have been associated with diverse molecular processes and pathways, and the molecular underpinnings of LTP on the time scales of a few minutes or of several hours are well established. However, the principles underlying the maintenance of the early phase of LTP (E-LTP) on the intermediate time scale of $1-6$ hours remains elusive. We hypothesize that specific features of postsynaptic receptor trafficking would be responsible for sustaining synaptic changes during this LTP phase. We test this hypothesis by formalizing a biophysical model that integrates several experimentally-motivated mechanisms. The model captures a wide range of experimental findings and predicts that synaptic changes are preserved for hours when the receptor dynamics are shaped by the interplay of structural changes of the spine in conjunction with increased trafficking from recycling endosomes and the cooperative binding of receptors. Furthermore, our model provides several predictions to verify experimentally our findings.

Significance Statement

The cognitive ability of learning is associated to plasticity-induced changes of the synaptic transmission efficacy that is mediated by AMPA receptors. Synaptic changes depend on a multitude of molecular and physiological mechanisms, building complex interaction networks. By formalizing and employing a biophysical model of AMPAR trafficking, we unravel and evaluate the interplay between key mechanisms such as receptor binding, exocytosis, morphological changes, or cooperative receptor binding. Our findings indicate that cooperative receptor binding in conjunction with morphological changes of the spine and increased trafficking from recycling endosomes leads to the maintenance of synaptic changes on behaviorally relevant time spans. Such a better understanding about the principles underlying synaptic changes might allow further insights into deficient plasticities that underlie neurodegenerative diseases.

Introduction

Synaptic plasticity adapts the synaptic transmission strength and is associated with cognitive processes such as learning and memory. For excitatory synapses the transmission strength is mainly determined by the number of AMPARs accumulating at the PSD (Anggono and Huganir, 2012; Lisman et al., 2012; Opazo et al., 2012; Choquet, 2018). LTP can be divided into different phases such as early-phase LTP (E-LTP) that is decayed after 1-6 hrs after induction or late-phase LTP (L-LTP), which lasts for several hours or even days and depends on the synthesis of new proteins (Frey and Morris, 1997; Abraham, 2003; Bliss et al., 2018). Although different molecular processes and pathways underlying the different phases of LTP, especially of L-LTP, have been identified (Malinow and Malenka, 2002; Abraham, 2003; Gallimore et al., 2018), the biological mechanisms maintaining E-LTP remain unclear. To address this issue, here we focus on the period after the induction of LTP, which is basically independent from protein synthesis, and investigate the influence of different experimentally motivated candidate mechanisms on the AMPAR dynamics at the PSD.

AMPARs are continuously inserted and removed from the spine membrane by exocytosis and endocytosis (Passafaro et al., 2001; Patterson et al., 2010; Kennedy et al., 2010; Choquet and Triller, 2013). Experimental studies indicate that E-LTP dissolves already after several minutes if the exocytosis of additional AMPARs is blocked (Penn et al., 2017; Kennedy et al., 2010; Wu et al., 2017; Lledo et al., 1998; Figure 1A, triangles). Although these results suggest that exocytosis could be the main mechanism underlying the maintenance of E-LTP, the rate of exocytosis events is only increased for a few minutes after LTP-induction (Patterson et al., 2010; Tanaka and Hirano, 2012; Figure 1B).

While AMPARs are regularly exchanged between the PSD, the postsynaptic and the extrasynaptic membrane via lateral diffusion they can become bound at the PSD to become functional (Borgdorff and Choquet, 2002; Tardin et al., 2003; Heine et al., 2008; Choquet and Triller, 2013). The binding is regulated by the phosphorylation of PSD proteins such as PSD95 (Opazo et al., 2012; Huganir and Nicoll, 2013;

MacGillavry et al., 2013). However, the phosphorylation of PSD proteins via kinases such as CaMKII is only upregulated for a few minutes after LTP-induction (Lee et al., 2009; Figure 1C) while concentrations of PSD proteins only increase in the presence of protein synthesis and persistent spine enlargement (Bosch et al., 2014; Meyer et al., 2014). Taken together, these results demonstrate that the principles underlying the maintenance of E-LTP remain unknown.

Besides exocytosis and trapping other biological mechanisms influence the AMPAR dynamics at the dendritic spine. For instance, the spine morphology regulates the translocation and dwell time of proteins at the spine's membrane and cytosol (Ashby et al., 2006; Kusters et al., 2013; Adrian et al., 2017; Bosch et al., 2014). LTP induction also triggers spine enlargment (so-called structural LTP (sLTP); Matsuzaki et al., 2004; Yang et al., 2008) and this enlargement (if protein synthesis is blocked) can last for as long as E-LTP (Bosch et al., 2014). Several experimental studies suggest that during sLTP Recycling Endosomes (REs) containing AMPARs are mobilized into the spine (Park et al., 2004, 2006; Wang et al., 2008). Exocytosis from these REs delivers AMPARs to the spine membrane, stabilizes the spine after LTP induction and has been suggested to be involved in the early maintenance of LTP (Park et al., 2004, 2006; Wang et al., 2008; Yang et al., 2008; Kneussel and Hausrat, 2016). Furthermore, AMPARs are not homogeneously distributed in the PSD but clustered (Nair et al., 2013; Hruska et al., 2018). The emergence of such clusters can be related to cooperative interactions between the receptors or between the receptors and scaffolding proteins, which in turn influence the binding of the AMPARs (Ranft et al., 2017; Shouval, 2005; Burlakov et al., 2012; Sekimoto and Triller, 2009; Shomar et al., 2017). The relation between morphological spine changes, trafficking from REs, AMPAR clustering and the induction and maintenance of E-LTP remains unexplained.

In this study, based on well-established theoretical studies (Earnshaw and Bressloff, 2006; Shomar et al., 2017) we derive a mathematical model of AMPAR trafficking in a dendritic spine that integrates diverse experimental data (Patterson et al., 2010; Yudowski et al., 2007; Matsuzaki et al., 2004; Yang et al., 2008; Park et al., 2006;

Nusser et al., 1998; Makino and Malinow, 2009; Frischknecht et al., 2009; Ehlers et al., 2007; Heine et al., 2008; Lee et al., 2009). We use this model to investigate systematically the impact of the different biological mechanisms discussed before on the maintenance of E-LTP by comparing the model data with the experimental data shown in Figure 1 (Barco et al., 2002; Lee et al., 2009; Patterson et al., 2010; Penn et al., 2017).

We find that the biological mechanisms of morphological changes in conjunction with increased RE trafficking and cooperative binding can complement each other and together provide a possible explanation for the decay time of E-LTP as well as the dependence of LTP on exocytosis. This combined model integrating AMPAR trafficking, morphological changes, and cooperative binding provides a new hypothesis about the principles underlying the maintenance of E-LTP and leads to specific, new experimental predictions that could verify our findings.

Materials and Methods

Basic model of AMPAR-trafficking

The basic model integrates the core processes of AMPAR trafficking in the dendritic spine: lateral diffusion to and from the dendritic membrane, exo- and endocytosis within the spine, and binding to and disassociation from scaffolding proteins in the PSD (Figure 5A). We formalize the coaction of these processes by considering the numbers of AMPARs that freely move on the membrane of the spine denoted by U and of AMPARs that are bound in the PSD labeled by B. The surface area of the spine is denoted by A_{spine}. Please note that we do not explicitly model the number of AMPARs being in the intracellular space of the spine or on the dendritic membrane, as the rate of exocytosis is slow (Passafaro et al., 2001; Patterson et al., 2010) and diffusion of surface receptors is fast (Tardin et al., 2003) we assume that the dendritic and intracellular pools are rapidly replenished. On the synaptic membrane, the number of free, unbound AMPARs is increased by exocytosis with rate $k_{exo}\, S_{RE}$ where S_{RE} denotes the size of an exocytic event, lateral diffusion from the dendritic

membrane to the spine with rate k_{in}, and AMPARs that are unbound from scaffolding proteins described by $k_{BU} \cdot B$. It is decreased by endocytosis with $k_{endo} \frac{U}{A_{spine}}$, lateral diffusion to the dendrite with $k_{out} \cdot U$, and AMPARs being bound in the PSD described by $k_{UB}(P - B) \frac{U}{A_{spine}}$ with number of slots P formed by scaffolding proteins. Thus, the change in the number of unbound AMPARs can be formalized by

$$\frac{dU}{dt} = k_{exo} S_{RE} + k_{in} + k_{BU} B - k_{endo} \frac{U}{A_{spine}} - k_{out} U - k_{UB}(P - B) \frac{U}{A_{spine}}. \quad (1)$$

We do not consider direct endo- and exocytosis of bound AMPARs such that its number is only regulated by the interchange with freely moving AMPARs.

$$\frac{dB}{dt} = k_{UB}(P - B) \frac{U}{A_{spine}} - k_{BU} B. \quad (2)$$

Equations 1 and 2 describe the AMPAR-dynamics on the spine's membrane under basal condition. We derived the corresponding set of parameter values of an average spine by estimating the values from several experimental studies that are mainly conducted in hippocampal cultures and slices (see Table 1) and are described in more detail below.

Parameter derivation

In this section we will explain the choice of values of the model parameters listed in Tables 1 and 2. We will denote parameter values under basal conditions, i.e. before LTP induction, by a superscript index 0.

The *number of AMPARs* in the PSD has been estimated to around $15 - 30$ receptors (Sheng and Hoogenraad, 2007; Cheng et al., 2006; Nusser et al., 1998; Nair et al., 2013; the maximum number could be up to 140 receptors (Matsuzaki et al., 2001; Nusser et al., 1998). The exact fraction of mobile receptors in the spine is unclear. While some studies report around 50% mobile receptors at spines (Tardin et al., 2003; Bats et al., 2007; Ashby et al., 2006; Petrini et al., 2009) more recent

studies show that $\approx 65 - 90\%$ of the AMPARs are confined in PSD nanodomains Lee et al., 2017; Nair et al., 2013. The question remains how many of these confined AMPARs are also contributing to the excitatory transmission or whether they functionally belong to the the mobile pool U in our model. Considering the above we here assume a total number of 30 AMPARs in the steady state with 2/3 bound receptors ($B^* = 20$) and 1/3 mobile receptors ($U^* = 10$); $*$ marks the steady state.

The *exocytosis rate* within spines has been measured by Patterson et al. (2010) who found ≈ 0.11 exocytosis events per minute under basal conditions (k^0_{exo}). Per event about 51±36 GluR1 subunits are released, as estimated in a study by Yudowski et al. (2007). We will denote the size of an exocytosis event under basal conditions by S^0_{RE}, which depends on the capacity of the spine to recycle AMPARs back to the spine membrane and therefore on the number and size of recycling endosomes in the periphery of the spine (Park et al., 2004; Wang et al., 2008). AMPARs are tetrameric, therefore this corresponds to $S^0_{RE} = 13 \pm 9$ AMPA receptors per event. Note that exocytosis events at spines might contain less receptors (Patterson et al., 2010), however, the overall rate of exocytosis might also be underestimated in these experiments (Hiester et al., 2018).

The *diffusion-dependent parameters* k_{out} and k_{in} are estimated from FRAP and receptor tracking experiments, assuming that the contribution of exocytosis to the fluorescence recovery is small (Patterson et al., 2010; Makino and Malinow, 2009; Passafaro et al., 2001). The recovery half time in these FRAP experiments ranges from 10s of seconds up to 100 s depending on the spine and AMPAR subunit type (Frischknecht et al., 2009; Makino and Malinow, 2009; Patterson et al., 2010; Ashby et al., 2006). We therefore estimate that diffusing AMPARs enter the spine's membrane from the dendrite at a rate of $k'_{in} \approx 0.02s^{-1}$. Given that receptor exchange occurs mainly due to diffusion (Patterson et al., 2010; Makino and Malinow, 2009), in- and efflux need to be properly balanced in accordance with the steady state value U^*. Therefore, we set $k_{in} = k'_{in} \cdot U^*$. Receptor tracking and theoretical studies reveal receptor dwell times in confined states at spines that are also on the order of

10s of seconds (Borgdorff and Choquet, 2002; Ehlers et al., 2007; Nair et al., 2013; Kusters et al., 2013). Thereby $k^0_{out} = k'_{in}$ is a convenient choice. In the following we will sometimes use the term dwell time $\tau_{dwell} = 1/k^0_{out}$.

The *unbinding rate* of AMPARs k_{BU} is estimated based on the dwell time of receptors being in an immobile state at the PSD. Given Heine et al. (2008), we set $k_{BU} = 1/10\, s^{-1}$. We assume that functional bound AMPARs need to be in an immobilized state, considering that precise alignment of AMPARs with the presynaptic active zone is important for excitatory synaptic transmission (Haas et al., 2018).

The number of binding sites or *slots* P contained in a PSD is not clear. However, the receptor number in spines is much smaller than the number of most scaffolding proteins being in the PSD (Sheng and Hoogenraad, 2007). Also, the EPSP amplitude increases by about $50 - 200\%$ during LTP-induction, indicating that the number of slots is at least three times higher than the number of bound receptors before induction. Therefore, we assume $P = 3.5 \cdot B^*$.

For the *spine volume* under basal conditions we assume $V^0_{spine} = 0.08 \mu m^3$ (Matsuzaki et al., 2004; Adrian et al., 2017). We calculate the surface area A^0_{spine} from the volume considering spherical spines heads.

Given that we set the number of AMPARs under basal conditions, the *endocytosis rate* k_{endo} and the *binding rate* k^0_{UB} (before LTP induction) can be calculated analytically from the fixed point equation of the basic model. For this, we rearrange the fixed point equations (derived by setting equations 1, 2 to zero) to solve for k_{endo} and k_{UB}:

$$k_{endo} = A^0_{spine} \frac{k^0_{exo} + k_{in} - k^0_{out} U^*}{U^*}, \tag{3}$$

$$k^0_{UB} = A^0_{spine} \frac{B^* k_{BU}}{(P - B^*)\, U^*}. \tag{4}$$

Parameter changes during LTP-induction

LTP-induction triggers a change in the exocytosis rate k_{exo} $(Events/s)$ and the binding rate k_{UB} (Patterson et al., 2010; Lee et al., 2009) (see Introduction and Fig. 1). The change in both parameters $k_x, x \in \{exo, UB\}$ during LTP-induction is modeled by the following functions:

$$k_x(t) = k_x^0 \cdot f(t, C_x = 1), \tag{5}$$

with

$$f(t) = \left(C_x + A_x \frac{e^{-t/\tau_x} - e^{-t/\tau_x^{increase}}}{A_{norm}} \right) \tag{6}$$

where

$$A_{norm} = \frac{\tau_x}{\tau_x^{increase}}^{\frac{\tau_x^{increase}}{\tau_x^{increase} - \tau_x}} - \frac{\tau_x}{\tau_x^{increase}}^{\frac{\tau_x}{\tau_x^{increase} - \tau_x}} \tag{7}$$

is a normalizing factor, such that $max((exp(-t/\tau_x) - exp(-t/\tau_x^{increase}))/A_{norm}) = 1$. A_x is the factor by which the parameter changes during LTP-induction. τ_x and $\tau_x^{increase}$ are time constants for the decay and increase respectively. Upon LTP-induction the exocytosis rate increases 5-fold for the duration of the stimulus ($\approx 1min.$), as shown in 2-photon-glutamate-uncaging experiments (Patterson et al., 2010). We therefore assume a rapid increase in the exocytosis rate k_{exo} with a time constant $\tau_{exo}^{increase} = 25s$ during E-LTP-induction and a decay with a time constant of $\tau_{exo} = 60s$. Based on Patterson et al. (2010); Kennedy et al. (2010), we set $A_{exo} = 5$.

We also assume an increase in the binding rate k_{UB}. Several PSD scaffolding and auxiliary proteins, such as PSD95 and Stargazin that are targets of the kinase CaMKII, are important for anchoring receptors at the PSD (Opazo et al., 2010; Bats et al., 2007; Schnell et al., 2002; Ehrlich and Malinow, 2004; Nair et al., 2013). Upon 2-photon glutamate uncaging, CaMKII activity rapidly increases but decreases within $2min.$ Lee et al. (2009); Chang et al. (2017). We therefore assume a brief increase in the binding rate ($\tau_{UB}^{increase} = 5s$) and a slower decay ($\tau_{UB} = 60s$). We have no reference point for the change in amplitude of k_{UB}. Thus, we assume that it increases high enough to nearly saturate the available slots, which is the case for $A_{UB} = 30$.

Computer simulation and random sampling of the parameter space

For each model version we used the classical Runge-Kutta method to solve the corresponding set of differential equations.

In addition to the parameter estimates from above we randomly sampled parameter (Figures 8 and 9) to evaluate within which parameter regime the model can be matched to the experimental data of E-LTP with and without exocytosis. In this method, parameters of the model are chosen randomly within a predefined regime (Table 3). The outcome of a simulation is compared to the reference experimental data using the following cost function:

$$\Delta x = \frac{1}{T}\left(\int_0^T |B_{ref}^{E-LTP} - B_{sim}^{E-LTP}|dt + \int_0^T |B_{ref}^{k_{exo}=0} - B_{sim}^{k_{exo}=0}|dt\right), \tag{8}$$

where B_{ref}^{E-LTP} (with exocytosis), $B_{ref}^{k_{exo}=0}$ (without exocytosis) are the reference data we match the model to and T is the duration of measurements. The cost function can be interpreted as the time averaged difference in the number of bound receptors between modeling and experimental data. We considered 2000 trials (different sets of parameter values) and evaluated the best 1%, according to the cost function.

We used as reference the experimental data from Barco et al. (2002) and Penn et al. (2017) (E-LTP, LTP with blocked exocytosis; Figure 1A), which is given in percentage of the baseline EPSPs. We fitted the EPSP data by the following function:

$$\begin{aligned} EPSP_x(t) = f(t, C_{x,short}, A_{x,short}, T_{x,short}, T_{x,short}^{increase}) \\ + f(t, C_{x,long}, A_{x,long}, T_{x,long}, T_{x,long}^{increase}), \end{aligned} \tag{9}$$

where $f(\cdot)$ is defined by Equation 6 and $x \in \{E-LTP, k_{exo}=0\}$. The function $EPSP_x(t)$ accounts for a short initial phase as well as for a subsequent long lasting phase. The fitted parameter values are listed in Table 4. We transferred this data from % of baseline EPSPs into units of receptor numbers by assuming the same baseline number of receptors for the reference as we did for the model (B^*, U^*,

$B_{ref}^{x} = \frac{EPSP^{x}(t)}{100\%} \cdot B^{*})$.

Modeling sLTP and RE trafficking

Structural long-term potentiation (sLTP) of the spine has been observed in several studies (Matsuzaki et al., 2001, 2004; Tanaka et al., 2008; Yang et al., 2008) and does depend on exocytosis from REs (Park et al., 2006; Yang et al., 2008). Similar to functional LTP, sLTP can be divided into different phases. Directly after the induction of sLTP the spine volume rapidly increases and subsequently decays (V_{spine}^{short}) but settles at a level above the original baseline V_{spine}^{long}. This late phase of sLTP depends on protein synthesis (Bosch et al., 2014, Figure 2A, black circles) and, if protein synthesis is blocked, V_{spine}^{long} decays. The decay time, however, differs between studies (Bosch et al., 2014; Tanaka et al., 2008; Yang et al., 2008). Based on the results from Yang et al. (2008), showing that functional LTP and sLTP decay with similar time constants in the presence of Anisomycin, and from Bosch et al. (2014), who found a slow spine volume decay over the time course of $2hrs$ after blocking protein synthesis, we assume that in the absence of protein synthesis sLTP decays with a time constant close to that of E-LTP (Figure 2A, purple line). In line with the results from Park et al. (2006), Yang et al. (2008) also found that sLTP occurs but rapidly decays if exocytosis is blocked with Botox (Figure 2A, black squares). Furthermore, several experiments suggest that the long-term spine enlargement triggered by LTP-induction ΔV_{spine}^{long} is correlated to the the initial spine volume V_{spine}^{0} (Matsuzaki et al., 2004; Tanaka et al., 2008; Yang et al., 2008)). We fitted the data by an exponential function (Figure 2B):

$$\Delta V_{spine}^{long} = \frac{a \cdot e^{V_{spine}^{0}/b} + c}{100\%} \tag{10}$$

with parameter values given in the legend of Figure 2B. Based on the findings discussed above, we formalized a model of the spine volume change that accounts

for all these observations:

$$V_{spine}(t) = V^0_{spine} \cdot \Big(f(t, 1, 1 + 1.75 \cdot \Delta V^{long}_{spine}, T_1, T_2^{increase}) + f(t, 0, V^{long}_{spine}, T_3, T_4^{increase}) \Big), \tag{11}$$

where $f(\cdot)$ is defined by Equation 6. The first term on the right hand site describes the initial, transient phase of structural plasticity V^{short}_{spine} that decays within $20min$. The amplitude of ΔV^{short}_{spine} depends on ΔV^{long}_{spine}, but it has a lower limit in the absence of a late phase (Matsuzaki et al., 2004). This property is described by $1 + 1.75 \cdot \Delta V^{long}_{spine}$. The time constants for the exponential increase and decay are $T_2^{increase} = 5s$, $T_1 = 250s$. The second term on the right hand side describes the long lasting second phase V^{long}_{spine} with a rise time constant $T_4^{increase} = 500$. The decay time is defined by the time constant T_3. When L-LTP is triggered, T_3 is very large, i.e. the spine volume does not decay over the time course of hours. In the absence of L-LTP, we set $T_3 = 50min$, which is the decay time constant of E-LTP (Figure 2A, purple line). If exocytosis is blocked, ΔV^{long}_{spine} is set to zero (Figure 2A, orange line).

The mean dwell time of proteins on the spine's membrane depends linear on the surface area of the spine (Schuss et al., 2007). Therefore,

$$k_{out} = \frac{A^0_{spine}}{A_{spine}} \cdot k^0_{out}, \tag{12}$$

where A^0_{spine} is the spine surface before LTP induction. We assume no change in the AMPAR diffusion coefficient. Equation 12 also ensures that the concentration of mobile AMPARs recovers after the increase of the spine surface area. Several studies have highlighted the importance of endosomal trafficking in LTP (Park et al., 2004, 2006; Wang et al., 2008; Zheng et al., 2015; da Silva et al., 2015; Kneussel and Hausrat, 2016). REs frequently move in and out of spines and are mobilized into the spine during LTP to deliver AMPARs (Wang et al., 2008; Park et al., 2006). Importantly this process does not depend on protein synthesis (Park et al., 2004). The number of REs in the spine increases after LTP induction and their size is increased even 30 min. after LTP induction (Park et al., 2006). In addition, ongoing

exocytosis from REs at spines is necessary to maintain the spine morphology and the spine size is correlated with the amount of local REs Park et al. (2006); Yang et al. (2008) suggesting a correlation between RE trafficking and spine volume. Also, correct positioning of REs at spines is important for LTP (da Silva et al., 2015) and theoretical studies suggest an important role of the locus of exocytosis being at the spine (Kusters et al., 2013; Czondor et al., 2012). In total, the above results suggest a close link between of RE positioning at spines, sLTP and the delivery of AMPARs. Therefore, while the number of AMPAR exocytosis events per minute only increases briefly after LTP induction (Patterson et al., 2010; Tanaka and Hirano, 2012), we hypothesize that the size of the single exocytosis event S_{RE} increases proportional to the spine volume. We describe the dynamics of the RE size inside the spine by

$$\frac{dS_{RE}}{dt} = k_{in}^{RE} - k_{out}^{RE}\, S_{RE}, \tag{13}$$

with

$$k_{out}^{RE}(t) = \frac{k_{out}^{RE\prime}\, V_{spine}^{0}}{V_{spine}(t)}, \tag{14}$$

where we set $k_{in}^{RE} = 0.1s^{-1}$. From the fixed point equation of 13 we derive $k_{out}^{RE\prime} = k_{in}^{RE}/S_{RE}^{*}$ (where $S_{RE}^{*} = S_{RE}^{0}$, see section on parameter derivation).

Cooperative binding model

Thanks to super resolution microscopy techniques like STORM and STED, in recent years, several studies revealed that synaptic proteins in the PSD are not homogeneously distributed but often clustered in so-called nanodomains (MacGillavry et al., 2013; Nair et al., 2013; Compans et al., 2016; Hruska et al., 2018). Several theoretical studies identified that such nanodomains emerge due to cooperative binding of proteins (Shouval, 2005; Burlakov et al., 2012; Sekimoto and Triller, 2009; Haselwandter et al., 2011; Ranft et al., 2017; Shomar et al., 2017). In this study we use the term cooperative binding to summarize the effects that neighboring receptors or scaffolding proteins have on the probability of (un-)binding of a receptor (red arrows in Figure 5E). In the following, we extend the basic model by cooperative binding of

AMPARs in the PSD. For this, we utilize a recent theoretical model capturing the essence of cooperativity given a few general assumptions (Shomar et al., 2017) (In the original study this model has been used to describe cooperativity between PSD scaffolding proteins not receptors). In our adaptation of this model the scaffolding proteins or slots are spatially organized on a grid (Figure 4A) where each mobile receptor U binds to a free slot with a certain rate dependent on the number of occupied nearest-neighbor slots (Eq. 15). Similarly, the rate of unbinding decreases with more bound receptors B being in the surrounding (Eq. (16)). Note that in this model the grid size ($N \times N$) is analog to P in the basic model (Equations 1 and 2.

$$\hat{k}_{UB}^{coop} = k_{UB}(\alpha\chi + 1)U \tag{15}$$

$$\hat{k}_{BU}^{coop} = k_{BU}(1 - \chi). \tag{16}$$

Here, χ is the fraction of occupied nearest neighbours on the grid (i.e. $n/8$ with $n = 0, 1, ..., 8$) and α is a measure for the cooperativity, where a big value coincides with a stronger influence of cooperativity. As apparent from Equations 15 and 16, the cooperative binding and unbinding rate $\hat{k}_{UB}^{coop}$, $\hat{k}_{BU}^{coop}$ change depending on the number of bound receptors on the grid and depending on the size of the grid P. We chose $k_{UB} = 0.0004(\#s)^{-1}$, $\alpha = 16$ and $k_{BU} = 0.1s^{-1}$. Note that the choices for k_{UB} and k_{BU} do not influence the dependence of $\langle\hat{k}_{UB}^{coop}\rangle$ or $\langle\hat{k}_{BU}^{coop}\rangle$ on P or B, where $\langle.\rangle$ denotes the mean rate per receptor across the grid and across many trials:

$$\langle\hat{k}_{UB}^{coop}\rangle = \frac{1}{\Delta t \cdot U \cdot (P - B)} \sum_{grid=0} \sum_{trials} p_{UB}^{coop}, \tag{17}$$

$$\langle\hat{k}_{BU}^{coop}\rangle = \frac{1}{\Delta t \cdot B} \sum_{grid=1} \sum_{trials} p_{BU}^{coop}, \tag{18}$$

where $grid = 0$ and $grid = 1$ denote the elements of the grid that are empty or occupied respectively. We did a stochastic simulation of this model (as in Shomar et al., 2017) with the binding and unbinding probabilities being $p_{UB}^{coop} = \hat{k}_{UB}^{coop} \cdot \Delta t$ and

$p_{BU} = \hat{k}_{BU}^{coop} \cdot \Delta t$ with the integration time step $\Delta t = 0.5s$. In addition, we describe U by

$$dU = (k_{in} - k_{out} \cdot U)dt + dB_{off} - dB_{on}, \tag{19}$$

where dB_{off} and dB_{on} are the receptors unbinding/binding from/to the grid respectively within one time step of the stochastic simulation. For the in- and efflux of mobile receptors we neglect the detailed dynamics of exocytosis and endocytosis (Equation 1). The efflux via lateral diffusion we keep the same as in the basic model ($k_{out} = 0.02s^{-1}$). To control the number of mobile receptors and thereby also the number of bound receptors on the grid, we vary the influx $k_{in} = k'_{in} \cdot U^*$ by varying U^* between $5-60$ with $k'_{in} = 0.02s^{-1}$. For the stochastic model we use $p_{out} = k_{out}\Delta t$ and $p_{in} = k_{in}\Delta t$.

To integrate the key principles of the cooperative model into the basic model of AMPAR-dynamics (Equations 1 and 2), we evaluated several iterations of the cooperative model for different numbers of available receptors U and slots P (grid size). From these, we obtained the mean binding $\langle \hat{k}_{UB}^{coop} \rangle$ and unbinding rate $\langle \hat{k}_{BU}^{coop} \rangle$ per mobile/bound receptor averaged across the grid and their dependency on number of slots P and bound receptors B (Figure 4B). We then formalized this dependency of binding and unbinding rate by fitting $\langle \hat{k}_{UB}^{coop} \rangle$ and $\langle \hat{k}_{BU}^{coop} \rangle$ by the following functions (Figure 4B dashed lines):

$$\frac{k_{BU}^{coop}}{k_{BU}} = \frac{\lambda(P)}{\beta(P) + B} - 0.5, \tag{20}$$

$$\frac{k_{UB}^{coop}}{k_{UB}} = m(P)B^{0.8} + 1 \tag{21}$$

with functions

$$\beta = m_\beta P + c_\beta, \tag{22}$$

$$\lambda = m_\lambda P + c_\lambda, \tag{23}$$

$$m = a_m/(P + b_m). \tag{24}$$

$\beta(P)$, $\lambda(P)$ and $m(P)$ are shown in Figure 3A-C. By this, we eliminate the spatial component of the cooperative binding model and obtain a description that we can integrate into our basic model by substituting k_{UB} and k_{BU} in Equations 1 and 2 by k_{UB}^{coop} and k_{UB}^{coop} (Figure 4B).

We find that the mean number of bound receptors B increases approximately linear with P, where the slope depends on the number of mobile receptors U (Figure 3D). Also the average number of clusters on the grid (more than 5 occupied slots that are direct neighbours) depends on U (Figure 3E). For $U^* < 15$, we find almost no clusters, but for $U^* = 15$ the number of clusters increases with P. For $U^* = 40$, the PSD is always densely occupied, therefore only one big cluster is found.

Endocytosis and binding rate in the steady state in the cooperative binding model

The dynamics of cooperative binding changes the steady state of the system. This implies that the endocytosis and the binding rate have to be derived from the the adapted fixed point equations resulting to:

$$k_{endo} = A_{spine}^0 \frac{k_{exo}^0 + k_{in} - k_{out}^0 U^*}{U^*}, \tag{25}$$

$$k_{UB}^0 = A_{spine}^0 \frac{B^* k_{BU}(b_m + P)\,(0.5(B^* + c_\beta + m_\beta P) - (c_\lambda + m_\lambda P))}{(B^* - P)\,(B^* + c_\beta + m_\beta * P)\,(a_m (B^*)^{0.8} + (b_m + P))U^*}. \tag{26}$$

Code Accessibility

The code will be published on GitHub after publication.

Results

The impact of increased exocytosis and binding rate on the maintenance of E-LTP

To examine whether the brief increase in exocytosis rate and CaMKII activity accounts for the maintenance of E-LTP for several hours, we first study a basic model of AMPAR trafficking.

We model the LTP-induced variation of the exocytosis and binding rate (Figure 1) by time-dependent functions of the related parameters (k_{exo} and k_{UB}; see Materials and Methods). Each function consists of two exponential functions with a maximum factor of increase (A_{exo} for exocytosis and A_{UB} for binding rate; see Table 2), a time scale of exponential increase ($\tau_{exo}^{increase}$, $\tau_{UB}^{increase}$), and a time scale of exponential decay (τ_{exo}, τ_{UB}) back to the level under basal condition (k_{exo}^{0}, k_{UB}^{0}). Please note that the extensions of the basic model to also include morphological and RE trafficking changes or cooperative receptor binding are described in the corresponding sections below.

Under basal condition, the different processes of AMPAR-dynamics described before balance each other such that the number of mobile and bound AMPARs in the PSD and on the synaptic membrane reach an equilibrium state of constant temporal averages with 28.5% of slots being occupied.

The induction of LTP and the related increase in exocytosis and binding rate lead to a fast increase in the number of mobile and bound AMPARs, which results in a stronger synaptic transmission strength (Figure 5B, blue). After a few minutes, the exocytosis and binding rate are back to the basal level (Figure 1B,C). Given these dynamics, in the basic model the increased level of bound AMPARs in the PSD declines such that it reaches the pre-LTP level after about $10 - 15$ minutes. This result indicates that some core mechanisms are missing, which maintain bound AMPARs in the PSD for a longer duration.

The influence of sLTP and RE trafficking

In addition to changes in exocytosis event and binding rate, the induction of LTP also yields structural modifications of the spine volume which is linked to increased trafficking of AMPAR containing REs into the spine Park et al. (2006, 2004); Wang et al. (2008); Zheng et al. (2015). Trafficking from REs has been hypothesized to be especially involved in the maintenance of E-LTP (Kneussel and Hausrat, 2016). Importantly, structural changes of the spine and the REs last much longer (Matsuzaki et al., 2004; Yang et al., 2008; Bosch et al., 2014; Park et al., 2006) than changes in the rate of exocytosis events (Patterson et al., 2010; Tanaka and Hirano, 2012) and exocytosis from REs is necessary to maintain the spine morphology (Park et al., 2006; Yang et al., 2008). Therefore, to account for the increased RE trafficking, we hypothesize that the size of exocytosis events increases proportional to the spine volume during E-LTP (for details see Materials and Methods).

All parameters of sLTP are based on previous studies (Bosch et al., 2014; Matsuzaki et al., 2004; Adrian et al., 2017; Yang et al., 2008; see Materials and Methods). Besides the morphological and RE dynamics, all model parameters are the same as for the basic model. Temporal changes of the exocytosis event size S_{RE} and the spine volume V_{spine} (Figure 6) influence the AMPAR-dynamics at the PSD (Figure 5C). Considering these functional relations in the model yields a different temporal development of the level of bound AMPARs in the PSD (Figure 5D, blue line) compared to the basic model (Figure 5B). Similar to the basic model, the induction of LTP leads to a strong and fast increase in the number of bound AMPARs; however, the level of bound AMPARs falls significantly slower with sLTP than in the basic model. This slow decay is much faster, if exocytosis is blocked (Figure 5D, orange line) and, given normal conditions, the time span until the AMPARs level falls back to the basal level is similar to experiments ($\approx 100min$; compare blue line to square data points). However, between 10 and 100 minutes the overall level of bound AMPARs is too low compared to the experimental data. Thus, the influence of the morphological changes of the spine head and increased trafficking from REs on the AMPAR-dynamics are not sufficient to explain the maintenance of E-LTP.

The influence of cooperative binding of receptors on AMPAR-dynamics

Our model of cooperative AMPAR-dynamics (Equations 1, 2 and 20, 21; based on (Shomar et al., 2017)) enables us to investigate the influence of cooperative binding effects on the maintenance of E-LTP. Like before, all parameters are taken from experiments and LTP-related changes of the exocytosis and binding rate are modelled by temporal variations of k_{exo} and k_{UB}. Similar to the basic model, LTP-induction yields a fast increase of the number of bound AMPARs followed by a fast decay (Figure 5F, blue line). Compared to the basic model, the decay is a bit slower such that the level of bound AMPARs reaches the basal condition after $\approx 30 - 35$ minutes; however, it is significantly faster than in experiments. The blockage of exocytosis, after LTP-induction, leads to a level of bound AMPARs significantly below the state under basal condition (orange line), which is different to the basic model or model of morphological and RE trafficking changes. This effect of reduced transmission strength is also found in experiments (triangles). Thus, also the cooperative effects between receptors is not sufficient to explain the maintenance of E-LTP. Interestingly, our simulations of the clustering on a grid model show that receptors at the core of a cluster have much longer dwell times than those a the border (Figure 7B). This could explain the discrepancy between the small dwell time of immobile receptors observed in receptor tracking experiments (Heine et al., 2008) and the slow fluorescence recovery of a presumable immobile pool in FRAP experiments (Makino and Malinow, 2009; Ashby et al., 2006).

Parameter variation

Although based on experimental data, the parameters considered before could embrace an imprecision in their exact values. We therefore utilize the random sampling method (see Materials and Methods) to find the parameter set that results in the best match of the AMPAR-dynamics of the model with the experimentally measured temporal course of transmission strength (Figure 1A). For this, we randomly drew 2000 times different parameter values of the LTP-induced temporal development of

the exocytosis (k^0_{exo}, τ_{exo}, A_{exo}) and the binding rate (k^0_{UB}, τ_{UB}, A_{UB}) from a reasonable regime (see Table 3) and simulated the resulting AMPAR-dynamics for the basic model and its extensions by morphological changes and RE trafficking (sLTP) or cooperative binding discussed before. To find the best match, for each trial we use a distance measure (Equation 8) between the temporal development of the number of bound AMPARs in the model and the experimentally measured development of the EPSP with and without blockage of exocytosis (see Materials and Methods).

Indeed, for all three model versions several parameter sets yield dynamics that are in agreement with experimental findings with and without the blockage of exocytosis (Figure 8A, colored lines; the 1% best matching parameter sets are shown). Furthermore, the temporal development of the binding rate is consistent with the CaMKII activity during LTP-induction (Figure 8B). However, for the basic model and the sLTP-model, the exocytosis rate becomes much too high compared to experiments and the decrease becomes too slow (Figure 8C). For the model of AMPAR-dynamics with cooperative binding the exocytosis rate stays in a reasonable regime but also decays too slowly (lime green). However, the latter result indicates that the increase in exocytosis due to RE trafficking might be sufficient to maintain E-LTP in the cooperative binding model.

We repeated this procedure for three different values of the number of bound and mobile AMPARs under basal condition (B^*, U^*) and of the dwell time of receptors in the spine (τ_{dwell}; Figure 9). As shown in Figure 8B, all model versions matching the experiments have parameter values of the binding rate being similar to experimental estimates. Therefore, in the following we will focus on the development and parameters of exocytosis such as the maximum value of the increase of the exocytosis rate (amplitude of exocytosis k^A_{exo}). For the basic model and its extension by sLTP, the baseline exocytosis rate k^0_{exo} (Figure 9A,B) and the amplitude of exocytosis increase during LTP-induction k^A_{exo} (Figure 9D,E) depend on the dwell time and the number of bound AMPARs under basal condition. They only match experimental values (indicated by red area) for small numbers of bound AMPARs ($B^* = 5$) and long dwell times ($\tau_{dwell} = 100s$). The AMPAR-dynamics including cooperative

effects lead to exocytosis rate parameters that match experimental values for all levels of steady state bound AMPARs and dwell times above $20s$ (Figure 9C,F). However, for all combinations of different parameter values, all three model versions of AMPAR-dynamics result to a significantly too slow decay of the exocytosis rate after LTP-induction (τ_{exo}).

Morphological changes and cooperative binding complement each other to maintain synaptic potentiation

We have shown that neither the basic AMPAR dynamics nor its extension by sLTP and RE trafficking or cooperative binding seem to explain the maintenance of E-LTP. Next, we test whether a combination of cooperative binding, sLTP and increased RE-trafficking (Figure 10A) complement each other to mediate E-LTP as observed experimentally. All model parameters and the temporal developments of exocytosis, binding rate, and spine volume are the same as before (Figure 5). In this combined model with experimentally derived parameters, the number of bound AMPARs increases rapidly after LTP induction (Figure 10B). If exocytosis is blocked, this increase is followed by a rapid decay below the baseline level (orange line). In presence of exocytosis, however, the combined dynamics of sLTP and cooperative binding sustains the level of bound AMPARs at a level that matches with the experimental data (blue line). But why are both mechanisms required to maintain E-LTP?

To provide an answer, we assume that the trafficking dynamics of AMPARs are much faster than the changes triggered by LTP. This allows us to consider the fixed point of bound AMPARs B^* as a function of the spine volume V_{spine} and respectively the size of exocytosis events S_{RE} (Figure 10C). This function illustrates the different influences cooperative binding, morphological changes and RE trafficking (Equation 13) have on the number of bound AMPARs:

- *Cooperative binding* influences the shape of this function. If the AMPAR dynamics are determined by cooperative binding (blue line), the function becomes steep and slightly sigmoidal-shaped. This is significantly different com-

pared to the function of the basic model, which has a shallow slope (black line).

- *Morphological changes* influence the argument of the function. A variation of the spine volume and the exocytosis event size shifts the system to a new state with a different number of bound AMPARs.

Thus, considering AMPAR-trafficking dynamics only extended by morphological changes and RE trafficking (black line) would imply that an increase by ΔS_{RE} results in a small change of the number of bound AMPARs. By contrast, if we additionally consider cooperative binding between AMPARs (blue line), a shift in V_{spine} and therefore in S_{RE} results in a significant increase of the number of bound receptors (here, ΔB). In other words, cooperative binding of AMPARs non-linearly amplifies the effect of morphological changes and RE trafficking.

For the results discussed before, we considered an average spine with a spine volume of $V^0_{spine} = 0.08\mu m^3$ before LTP-induction. Next, we evaluate to what degree E-LTP maintenance due to the combined dynamics depends on the spine size before LTP-induction, thus, on the initial volume V^0_{spine} with corresponding number of slots P. Experimental studies have shown that morphological changes mainly occur for small to intermediate spine sizes but not for large spines with volumes above about $0.3\mu m^3$ (Matsuzaki et al., 2004; Tanaka et al., 2008). To model this dependence of ΔV_{spine} on V^0_{spine}, we fitted the experimental data (Matsuzaki et al., 2004; Tanaka et al., 2008; Yang et al., 2008) by an exponential function (Figure 2B). The initial size of exocytosis events scales with the initial spine volume $S^0_{RE} = 13 \cdot V^0_{spine}/(0.08\mu m^3)$ in keeping with previous parameter choices. In addition, we assume that the number of slots P in the PSD depends linearly on the initial surface area of the spine A^0_{spine}:

$$P = P^{basal} \cdot \frac{A^0_{spine}}{A^{basal}_{spine}}, \tag{27}$$

where $P^{Basal} = 70$ and $A^{basal}_{spine} = 0.898\mu m^2$ such that the parameter values used before still hold (Table 1). By integrating the $\Delta V_{spine}(V^0_{spine})$ function and Equation 27 into the combined model, we can now consider different initial spine sizes and investigate the resulting maintenance of E-LTP. We find that E-LTP is sustained

for spines with an intermediate spine size before LTP-induction (Figure 10D). For large spines ($V^0_{spine} \gtrsim 0.35\mu m^3$), E-LTP is already dissolved after about 35 minutes matching experimental insights indicating that large spines do not experience long lasting LTP (Matsuzaki et al., 2004; Tanaka et al., 2008). For very small spines ($V^0_{spine} \lesssim 0.03\mu m^3$), E-LTP also dissolves after several minutes as the PSD contains only few binding sites and is too small for cooperativity between receptors to have a strong effect.

Model predictions

This study yields some experimentally verifiable predictions.

Our main prediction is the requirement of the interplay between cooperative binding of receptors and morphological spine changes accompanied by an increase in AMPAR trafficking to the spine surface from REs (Figure 10). By contrast, each mechanism alone does not lead to the required accumulation of bound receptors for a time span of several hours (Figure 5). We predict that due to cooperative effects increased exocytic trafficking of AMPARs is already sufficient for synaptic potentiation without the need for additional factors that stabilize AMPARs at the PSD (Figure 10C). The clustering model further implies that receptors are differently stabilized depending on their location within clusters with long dwell times of receptors at a cluster core but short dwell times at the border (Figure 7). This allows for an ongoing, rapid exchange of receptors that has been shown to benefit the recovery from depression after high frequency stimulation (Heine et al., 2008) but also implies the need for a sustained pool of extrasynaptic receptors that constantly replenishes receptors unbinding form the PSD scaffold. We thereby predict that the overall stability of the immobile pool depends on its size and the size of the spine's mobile pool respectively. Further, we propose that functional LTP saturates because large spines do not show long-lasting sLTP and thus we suggest no sustained increase in RE trafficking (Figure 10D). Thereby, E-LTP is not maintained long enough for L-LTP to evolve. We find that there exist three alternative explanations for the dependence of E-LTP on exocytosis: E-LTP is maintained by 1) stabilization of re-

ceptors due to an exocytic factor (Hiester et al., 2018), by 2) an exocytic factor that raises the probability of receptor binding or by 3) a rapid increase in the number of slots after LTP induction (Nicoll, 2017; Herring and Nicoll, 2016). If receptors are stabilized by an exocytic factor, we would expect that the dwell time of receptors in the immobilized state increases after LTP induction independent of their location which is different from the here proposed model where receptor immobilization depends on cooperativity and therefore on the receptors local environment . Most apparent, neither the generation of additional binding sites nor the exocytosis of factors that stabilize AMPARs require an increase in the concentration of the spine's mobile receptor pool to maintain E-LTP while in our model the mobile pool concentration needs to grow by $\approx 25\%$ (Figure 6A). Anyhow, the presented predictions require more experimental research to identify the different principles underlying long-term potentiation. It is unclear whether E-LTP is sustained if exocytosis is blocked shortly after LTP induction and similarly whether sustained exocytosis is needed for receptor stabilization. Also, how receptor mobility change in the long term after LTP-induction (10s of minutes to hours) and whether exocytosis of AMPARs or other cargo is necessary for E-LTP is still ambiguous (Hiester et al., 2018; Nicoll, 2017; Choquet, 2018).

Discussion

The question of how E-LTP is maintained has not clearly been answered in previous studies. Also, the role of receptor exocytosis is still ambiguous. In this study, we focused on two major experimental observations: First, E-LTP can be long lasting with decay times on the order of hours (Frey and Morris, 1997; Redondo and Morris, 2010). Second, there exists a strong dependency between LTP and exocytosis, although the exocytosis of AMPARs is slow compared to the rapid exchange of receptors via lateral diffusion (Penn et al., 2017; Wu et al., 2017; Lüscher et al., 1999; Passafaro et al., 2001; Patterson et al., 2010). Our model indicates that the experimentally observed increase in the rate of AMPAR exocytosis events and their binding to the PSD scaffold are not sufficient to maintain E-LTP (Fig-

ures 5, 8, and 9). Furthermore, our results indicate that sLTP accompanied by increased AMPAR trafficking from REs during E-LTP (Kneussel and Hausrat, 2016; Park et al., 2006; Lamprecht and LeDoux, 2004) and cooperative receptor binding (Shomar et al., 2017; Choquet, 2018) can individually also not account for the maintenance of E-LTP. However, we demonstrated and predict that cooperative receptor binding complemented by increased trafficking from REs is sufficient to sustain E-LTP. Thus, our study provides several insights about the functional roles of diverse mechanisms during LTP.

AMPAR number as an indicator for synaptic strength We assumed that the EPSP amplitude measured in LTP experiments is proportional to the number of bound AMPA receptors. This assumption is supported by several experimental studies demonstrating that LTP is mostly expressed at the postsynaptic site and that excitatory synaptic transmission depends on the number of AMPARs (Luscher and Malenka, 2012; Andrásfalvy and Magee, 2004; Collingridge et al., 2004; Isaac et al., 1995; Penn et al., 2017). However, several types of AMPARs have been identified that differently contribute to LTP and synaptic transmission (Zamanillo et al., 1999; Hayashi et al., 2000; Shi et al., 2001; Meng et al., 2003; Plant et al., 2006; Makino and Malinow, 2009; Isaac et al., 2007; Park et al., 2016). The overall conductance could be adapted by the insertion of different AMPAR types, each having a different conductivity (Benke and Traynelis, 2018). In addition, AMPARs already present at the PSD before induction might change their conductivity (Benke et al., 1998). Stargazin, for example, has been shown to enhance the glutamate affinity and conductance of AMPARs (Tomita et al., 2005a; Turetsky et al., 2005). By contrast, the results from Penn et al. (2017) indicate that the fast increase after LTP-induction is associated to binding of additional AMPARs and possibly not to changes of receptor conductivity. Thus, in this study we do not considered conductance changes of individual AMPARs. However, different levels of conductivity can be integrated into our model, for instance by weighting the contribution of a AMPAR to the synaptic strength, and by this the influence of temporal variations in the conductivity by the possible exchange of AMPAR types on LTP could be investigated.

AMPAR mobility We also assumed that AMPA receptors are transiently immobilized to become functional at the PSD and otherwise rapidly diffuse between spine and dendrite. This assumption is supported by several experimental studies (Opazo et al., 2012; Choquet, 2018; Hastings and Man, 2018). However, the experimental literature is not clear regarding the dwell time of immobilized receptors. Studies blocking exocytosis (Penn et al., 2017; Wu et al., 2017; Lüscher et al., 1999) show that LTP is very transient, which implies that newly bound AMPARs may unbind from binding sites within seconds or a few minutes and diffuse out of the PSD. In addition, single-receptor-tracking studies revealed AMPAR dwell times in immobilized or confined states on the order of seconds (Heine et al., 2008; Bats et al., 2007; Ehlers et al., 2007). However, the estimates from these studies are biased by the fact that receptors are tracked for only $60 - 200s$. In contrast, studies investigating the fluorescence recovery after photo-bleaching (FRAP) suggest that immobile receptors are trapped for $30min$ and longer (Makino and Malinow, 2009; Frischknecht et al., 2009; Ashby et al., 2006). However, it is not clear whether the pool of immobilized receptors measured in FRAP experiments is affected by LTP-induction. While one study (Makino and Malinow, 2009) found that the number of immobile GluR1, but not GluR2 increases after 2-photon glutamate uncaging, another study (Patterson et al., 2010) did not find a significant increase. Furthermore, single-receptor-tracking as well as FRAP experiments use probes, which could physically interact with the system and, thus, impede the evaluation of receptor dwell times. Interestingly, receptor clustering, as shown in this study, could account for both these observations as the dwell time depends on the specific physical position of the receptor within the PSD or nanodomain (Figure 7B).

In general, the detailed mechanisms underlying AMPAR trapping in the PSD remain unclear. Several studies have shown that AMPAR immobilization is mediated via the interaction with Stargazin, which binds with the scaffolding protein PSD95 (Opazo et al., 2010; Bats et al., 2007; Schnell et al., 2002; Nair et al., 2013). The interaction of Stargazin with PSD95 depends on its phosphorylation via CaMKII (Opazo et al., 2010; Tomita et al., 2005b). Therefore, we linked the mean CaMKII

activity in spines to the binding rate of AMPARs. As discussed before, the CaMKII activity decays back to its baseline level within minutes after LTP-induction (Figure 1C; Lee et al., 2009). However, a small part of CaMKII might be active for much longer periods of time by binding to a subunit of NMDA receptors (Barria and Malinow, 2005; Bayer et al., 2001; Sanhueza et al., 2011).

PSD growth during LTP We assumed no change in the number of binding sites during E-LTP, which is consistent with experimental observations showing that the PSD only increases in size about $50min$ after LTP induction and dependent on protein synthesis (Bosch et al., 2014). Also the number of PSD95 increases very gradually over the time course of 3 hours after LTP induction and only if the spine enlargement is stable (Meyer et al., 2014). However, it has been hypothesized that new binding sites may become available due to the unbinding of the protein SynGAP from PSD95 upon phosphorylation (Choquet, 2018; Nicoll, 2017). In addition, the CaMKII-NMDAR complex might mediate the composition of new binding sites (Sanhueza and Lisman, 2013). However, more data is required to quantify conclusively the influence of PSD changes on the maintenance of E-LTP.

Correlation between RE trafficking, structural and functional LTP The way in which sLTP, RE trafficking and functional LTP are interlinked is still ambiguous. Several experimental studies identified a correlations between the spine volume and the synaptic transmission (Matsuzaki et al., 2004; Yang et al., 2008; Matsuzaki et al., 2001). For instance, Matsuzaki et al. (2004) have shown that AMPAR-mediated currents and spine volume increase during LTP are correlated in the very early phase of LTP ($1 - 5min$) as well as at later stages ($> 30min$). These results indicate that the enlargement of the spine head might be an essential condition for the expression of LTP. In addition, exocytosis from REs is required for spine size maintenance (Park et al., 2006; Yang et al., 2008) and these are mobilized into the spine upon LTP-induction (Kneussel and Hausrat, 2016; Park et al., 2006, 2004; Wang et al., 2008). Also, exocytosis is required for sustained E-LTP (Penn et al., 2017). In this study we therefore use the spine volume as an indicator for the

number of AMPARs that are exocytosed from REs at the spine. However, how exactly the number of AMPAR exocytosed within one membrane fusion events scales with the size of the spine or of the spine's REs respectively is unclear and additional experimental data is needed. Also it is unclear whether exocytosis of AMPARs or of other cargo is the major factor shaping receptor accumulation (Hiester et al., 2018) and it has been suggested that REs might be involved in the regulation of synaptic PSD-95 levels rather than of the endocytic recycling of AMPARs (da Silva et al., 2015). In addition, there have been conflicting results regarding the impact of REs during the initial phase of sLTP (da Silva et al., 2015; Park et al., 2006). Spine growth in the absence of functional LTP has been observed in a study where an isolated GluR1 C-tail (lacking the ion-channel function) was inserted at synapses (Kopec et al., 2007). Also, LTD can be independent of the spine size, but not actin remodelling (b. Wang et al., 2007). Further work is needed to resolve some of the conflicting results and open questions regarding the trafficking of AMPARs and other proteins in synaptic function and plasticity.

Conclusion

In line with several other studies (Shouval, 2005; Burlakov et al., 2012; Shomar et al., 2017; Nair et al., 2013; Kusters et al., 2013; Wang et al., 2008; Park et al., 2004), our study supports the importance of cooperative binding, spine morphology and RE trafficking for LTP. Going further, our model predicts that cooperative binding and spine morphology complement each other to sustain E-LTP such that other phases or processes of (late-phase) LTP can set in. However, further experimental and theoretical studies are needed for the verification of the here derived predictions and conclusions. As discussed above, the processes involved in the control of AMPAR mobility and trapping and their relation to morphological spine changes and exocytosis still provide some unanswered questions. However, the model derived in this study provides a step allowing further investigations of these processes also with regard to other types of synaptic plasticity such as LTD and synaptic scaling or the role of different AMPAR types. Also, proper functioning of various types of synap-

tic plasticity is important for learning and memory and dysregulation of processes involved synaptic plasticity such as AMPAR trafficking have been implicated in different diseases such as Alzheimer and Epilepsy (Chater and Goda, 2014). However, to understand how deficits in receptor trafficking can evolve into neurodegenerative diseases we need to obtain a profound understanding of how different trafficking mechanisms can influence synaptic transmission.

References

Abraham, W. C. (2003). How long will long-term potentiation last? *Philosophical Transactions of the Royal Society of London. Series B: Biological Sciences*, 358(1432):735–744.

Adrian, M., Kusters, R., Storm, C., Hoogenraad, C. C., and Kapitein, L. C. (2017). Probing the interplay between dendritic spine morphology and membrane-bound diffusion. *Biophysical Journal*, 113(10):2261–2270.

Andrásfalvy, B. K. and Magee, J. C. (2004). Changes in AMPA receptor currents following LTP induction on rat CA1 pyramidal neurones. *The Journal of Physiology*, 559(2):543–554.

Anggono, V. and Huganir, R. L. (2012). Regulation of AMPA receptor trafficking and synaptic plasticity. *Current Opinion in Neurobiology*, 22(3):461–469.

Ashby, M. C., Maier, S. R., Nishimune, A., and Henley, J. M. (2006). Lateral diffusion drives constitutive exchange of AMPA receptors at dendritic spines and is regulated by spine morphology. *Journal of Neuroscience*, 26(26):7046–7055.

b. Wang, X., Yang, Y., and Zhou, Q. (2007). Independent expression of synaptic and morphological plasticity associated with long-term depression. *Journal of Neuroscience*, 27(45):12419–12429.

Barco, A., Alarcon, J. M., and Kandel, E. R. (2002). Expression of constitutively active CREB protein facilitates the late phase of long-term potentiation by enhancing synaptic capture. *Cell*, 108(5):689–703.

Barria, A. and Malinow, R. (2005). NMDA receptor subunit composition controls synaptic plasticity by regulating binding to CaMKII. *Neuron*, 48(2):289–301.

Bats, C., Groc, L., and Choquet, D. (2007). The interaction between stargazin and PSD-95 regulates AMPA receptor surface trafficking. *Neuron*, 53(5):719–734.

Bayer, K.-U., Koninck, P. D., Leonard, A. S., Hell, J. W., and Schulman, H. (2001). Interaction with the NMDA receptor locks CaMKII in an active conformation. *Nature*, 411(6839):801–805.

Benke, T. and Traynelis, S. F. (2018). AMPA-type glutamate receptor conductance changes and plasticity: Still a lot of noise. *Neurochemical Research*, 44(3):539–548.

Benke, T. A., Lüthi, A., Isaac, J. T. R., and Collingridge, G. L. (1998). Modulation of AMPA receptor unitary conductance by synaptic activity. *Nature*, 393(6687):793–797.

Bliss, T. V., Collingridge, G. L., Morris, R. G., and Reymann, K. G. (2018). Long-term potentiation in the hippocampus: discovery, mechanisms and function. *Neuroforum*, 24(3):A103–A120.

Borgdorff, A. J. and Choquet, D. (2002). Regulation of AMPA receptor lateral movements. *Nature*, 417(6889):649–653.

Bosch, M., Castro, J., Saneyoshi, T., Matsuno, H., Sur, M., and Hayashi, Y. (2014). Structural and molecular remodeling of dendritic spine substructures during long-term potentiation. *Neuron*, 82(2):444–459.

Burlakov, V. M., Emptage, N., Goriely, A., and Bressloff, P. C. (2012). Synaptic bistability due to nucleation and evaporation of receptor clusters. *Physical Review Letters*, 108(2).

Chang, J.-Y., Parra-Bueno, P., Laviv, T., Szatmari, E. M., Lee, S.-J. R., and Yasuda, R. (2017). CaMKII autophosphorylation is necessary for optimal integration of ca 2+ signals during LTP induction, but not maintenance. *Neuron*, 94(4):800–808.e4.

Chater, T. E. and Goda, Y. (2014). The role of AMPA receptors in postsynaptic mechanisms of synaptic plasticity. *Frontiers in Cellular Neuroscience*, 8.

Cheng, D., Hoogenraad, C. C., Rush, J., Ramm, E., Schlager, M. A., Duong, D. M., Xu, P., Wijayawardana, S. R., Hanfelt, J., Nakagawa, T., Sheng, M., and Peng, J. (2006). Relative and absolute quantification of postsynaptic density proteome isolated from rat forebrain and cerebellum. *Molecular & Cellular Proteomics*, 5(6):1158–1170.

Choquet, D. (2018). Linking nanoscale dynamics of AMPA receptor organization to plasticity of excitatory synapses and learning. *The Journal of Neuroscience*, 38(44):9318–9329.

Choquet, D. and Triller, A. (2013). The dynamic synapse. *Neuron*, 80(3):691–703.

Collingridge, G. L., Isaac, J. T. R., and Wang, Y. T. (2004). Receptor trafficking and synaptic plasticity. *Nature Reviews Neuroscience*, 5(12):952–962.

Compans, B., Choquet, D., and Hosy, E. (2016). Review on the role of AMPA receptor nano-organization and dynamic in the properties of synaptic transmission. *Neurophotonics*, 3(4):041811.

Czondor, K., Mondin, M., Garcia, M., Heine, M., Frischknecht, R., Choquet, D., Sibarita, J.-B., and Thoumine, O. R. (2012). Unified quantitative model of AMPA receptor trafficking at synapses. *Proceedings of the National Academy of Sciences*, 109(9):3522–3527.

da Silva, M. E., Adrian, M., Schätzle, P., Lipka, J., Watanabe, T., Cho, S., Futai, K., Wierenga, C. J., Kapitein, L. C., and Hoogenraad, C. C. (2015). Positioning of AMPA receptor-containing endosomes regulates synapse architecture. *Cell Reports*, 13(5):933–943.

Earnshaw, B. A. and Bressloff, P. C. (2006). Biophysical model of AMPA receptor trafficking and its regulation during long-term potentiation/long-term depression. *Journal of Neuroscience*, 26(47):12362–12373.

Ehlers, M. D., Heine, M., Groc, L., Lee, M.-C., and Choquet, D. (2007). Diffusional trapping of GluR1 AMPA receptors by input-specific synaptic activity. *Neuron*, 54(3):447–460.

Ehrlich, I. and Malinow, R. (2004). Postsynaptic density 95 controls AMPA receptor incorporation during long-term potentiation and experience-driven synaptic plasticity. *Journal of Neuroscience*, 24(4):916–927.

Frey, U. and Morris, R. G. M. (1997). Synaptic tagging and long-term potentiation. *Nature*, 385(6616):533–536.

Frischknecht, R., Heine, M., Perrais, D., Seidenbecher, C. I., Choquet, D., and Gundelfinger, E. D. (2009). Brain extracellular matrix affects AMPA receptor lateral mobility and short-term synaptic plasticity. *Nature Neuroscience*, 12(7):897–904.

Gallimore, A. R., Kim, T., Tanaka-Yamamoto, K., and Schutter, E. D. (2018). Switching on depression and potentiation in the cerebellum. *Cell Reports*, 22(3):722–733.

Haas, K. T., Compans, B., Letellier, M., Bartol, T. M., Grillo-Bosch, D., Sejnowski, T. J., Sainlos, M., Choquet, D., Thoumine, O., and Hosy, E. (2018). Pre-post synaptic alignment through neuroligin-1 tunes synaptic transmission efficiency. *eLife*, 7.

Haselwandter, C. A., Calamai, M., Kardar, M., Triller, A., and da Silveira, R. A. (2011). Formation and stability of synaptic receptor domains. *Physical Review Letters*, 106(23).

Hastings, M. H. and Man, H.-Y. (2018). Synaptic capture of laterally diffusing AMPA receptors – an idea that stuck. *Trends in Neurosciences*, 41(6):330–332.

Hayashi, Y., Shi, S.-H., Esteban, J. A., Piccini, A., Poncer, J.-C., and Malinow, R. (2000). Driving AMPA receptors into synapses by LTP and CaMKII: Requirement for GluR1 and PDZ domain interaction. *Science*, 287(5461):2262–2267.

Heine, M., Groc, L., Frischknecht, R., que, J.-C. B., Lounis, B., Rumbaugh, G., Huganir, R. L., Cognet, L., and Choquet, D. (2008). Surface mobility of postsynaptic AMPARs tunes synaptic transmission. *Science*, 320(5873):201–205.

Herring, B. E. and Nicoll, R. A. (2016). Long-term potentiation: From CaMKII to AMPA receptor trafficking. *Annual Review of Physiology*, 78(1):351–365.

Hiester, B. G., Becker, M. I., Bowen, A. B., Schwartz, S. L., and Kennedy, M. J. (2018). Mechanisms and role of dendritic membrane trafficking for long-term potentiation. *Frontiers in Cellular Neuroscience*, 12.

Hruska, M., Henderson, N., Marchand, S. J. L., Jafri, H., and Dalva, M. B. (2018). Synaptic nanomodules underlie the organization and plasticity of spine synapses. *Nature Neuroscience*, 21(5):671–682.

Huganir, R. L. and Nicoll, R. A. (2013). AMPARs and synaptic plasticity: The last 25 years. *Neuron*, 80(3):704–717.

Isaac, J. T., Ashby, M. C., and McBain, C. J. (2007). The role of the GluR2 subunit in AMPA receptor function and synaptic plasticity. *Neuron*, 54(6):859–871.

Isaac, J. T., Nicoll, R. A., and Malenka, R. C. (1995). Evidence for silent synapses: Implications for the expression of LTP. *Neuron*, 15(2):427–434.

Kennedy, M. J., Davison, I. G., Robinson, C. G., and Ehlers, M. D. (2010). Syntaxin-4 defines a domain for activity-dependent exocytosis in dendritic spines. *Cell*, 141(3):524–535.

Kneussel, M. and Hausrat, T. J. (2016). Postsynaptic neurotransmitter receptor reserve pools for synaptic potentiation. *Trends in Neurosciences*, 39(3):170–182.

Kopec, C. D., Real, E., Kessels, H. W., and Malinow, R. (2007). GluR1 links structural and functional plasticity at excitatory synapses. *Journal of Neuroscience*, 27(50):13706–13718.

Kusters, R., Kapitein, L. C., Hoogenraad, C. C., and Storm, C. (2013). Shape-induced asymmetric diffusion in dendritic spines allows efficient synaptic AMPA receptor trapping. *Biophysical Journal*, 105(12):2743–2750.

Lamprecht, R. and LeDoux, J. (2004). Structural plasticity and memory. *Nat. Rev. Neurosci.*, 5:45–54.

Lee, S. H., Jin, C., Cai, E., Ge, P., Ishitsuka, Y., Teng, K. W., de Thomaz, A. A., Nall, D., Baday, M., Jeyifous, O., Demonte, D., Dundas, C. M., Park, S., Delgado, J. Y., Green, W. N., and Selvin, P. R. (2017). Super-resolution imaging of synaptic and extra-synaptic AMPA receptors with different-sized fluorescent probes. *eLife*, 6.

Lee, S.-J. R., Escobedo-Lozoya, Y., Szatmari, E. M., and Yasuda, R. (2009). Activation of CaMKII in single dendritic spines during long-term potentiation. *Nature*, 458(7236):299–304.

Lisman, J., Yasuda, R., and Raghavachari, S. (2012). Mechanisms of CaMKII action in long-term potentiation. *Nature Reviews Neuroscience*, 13(3):169–182.

Lledo, P.-M., Zhang, X., Südhof, T. C., Malenka, R. C., and Nicoll, R. A. (1998). Postsynaptic membrane fusion and long-term potentiation. *Science*, 279(5349):399–403.

Luscher, C. and Malenka, R. C. (2012). NMDA receptor-dependent long-term potentiation and long-term depression (LTP/LTD). *Cold Spring Harbor Perspectives in Biology*, 4(6):a005710–a005710.

Lüscher, C., Xia, H., Beattie, E. C., Carroll, R. C., von Zastrow, M., Malenka, R. C., and Nicoll, R. A. (1999). Role of AMPA receptor cycling in synaptic transmission and plasticity. *Neuron*, 24(3):649–658.

MacGillavry, H. D., Song, Y., Raghavachari, S., and Blanpied, T. A. (2013). Nanoscale scaffolding domains within the postsynaptic density concentrate synaptic AMPA receptors. *Neuron*, 78(4):615–622.

Makino, H. and Malinow, R. (2009). AMPA receptor incorporation into synapses during LTP: The role of lateral movement and exocytosis. *Neuron*, 64(3):381–390.

Malinow, R. and Malenka, R. C. (2002). AMPA receptor trafficking and synaptic plasticity. *Annual Review of Neuroscience*, 25(1):103–126.

Matsuzaki, M., Ellis-Davies, G. C. R., Nemoto, T., Miyashita, Y., Iino, M., and Kasai, H. (2001). Dendritic spine geometry is critical for AMPA receptor expression in hippocampal CA1 pyramidal neurons. *Nature Neuroscience*, 4(11):1086–1092.

Matsuzaki, M., Honkura, N., Ellis-Davies, G. C. R., and Kasai, H. (2004). Structural basis of long-term potentiation in single dendritic spines. *Nature*, 429(6993):761–766.

Meng, Y., Zhang, Y., and Jia, Z. (2003). Synaptic transmission and plasticity in the absence of AMPA glutamate receptor GluR2 and GluR3. *Neuron*, 39(1):163–176.

Meyer, D., Bonhoeffer, T., and Scheuss, V. (2014). Balance and stability of synaptic structures during synaptic plasticity. *Neuron*, 82(2):430–443.

Nair, D., Hosy, E., Petersen, J. D., Constals, A., Giannone, G., Choquet, D., and Sibarita, J.-B. (2013). Super-resolution imaging reveals that AMPA receptors inside synapses are dynamically organized in nanodomains regulated by PSD95. *Journal of Neuroscience*, 33(32):13204–13224.

Nicoll, R. A. (2017). A brief history of long-term potentiation. *Neuron*, 93(2):281–290.

Nusser, Z., Lujan, R., Laube, G., Roberts, J. B., Molnar, E., and Somogyi, P. (1998). Cell type and pathway dependence of synaptic AMPA receptor number and variability in the hippocampus. *Neuron*, 21(3):545–559.

Opazo, P., Labrecque, S., Tigaret, C. M., Frouin, A., Wiseman, P. W., Koninck, P. D., and Choquet, D. (2010). CaMKII triggers the diffusional trapping of surface AMPARs through phosphorylation of stargazin. *Neuron*, 67(2):239–252.

Opazo, P., Sainlos, M., and Choquet, D. (2012). Regulation of AMPA receptor surface diffusion by PSD-95 slots. *Current Opinion in Neurobiology*, 22(3):453–460.

Park, M., Penick, E. C., Edwards, J. G., Kauer, J. A., and Ehlers, M. D. (2004). Recycling endosomes supply AMPA receptors for LTP. *Science*, 305(5692):1972–1975.

Park, M., Salgado, J. M., Ostroff, L., Helton, T. D., Robinson, C. G., Harris, K. M., and Ehlers, M. D. (2006). Plasticity-induced growth of dendritic spines by exocytic trafficking from recycling endosomes. *Neuron*, 52(5):817–830.

Park, P., Sanderson, T. M., Amici, M., Choi, S.-L., Bortolotto, Z. A., Zhuo, M., Kaang, B.-K., and Collingridge, G. L. (2016). Calcium-permeable AMPA receptors mediate the induction of the protein kinase a-dependent component of long-term potentiation in the hippocampus. *Journal of Neuroscience*, 36(2):622–631.

Passafaro, M., Piëch, V., and Sheng, M. (2001). Subunit-specific temporal and spatial patterns of AMPA receptor exocytosis in hippocampal neurons. *Nature Neuroscience*, 4(9):917–926.

Patterson, M. A., Szatmari, E. M., and Yasuda, R. (2010). AMPA receptors are exocytosed in stimulated spines and adjacent dendrites in a ras-ERK-dependent manner during long-term potentiation. *Proceedings of the National Academy of Sciences*, 107(36):15951–15956.

Penn, A. C., Zhang, C. L., Georges, F., Royer, L., Breillat, C., Hosy, E., Petersen, J. D., Humeau, Y., and Choquet, D. (2017). Hippocampal LTP and contextual learning require surface diffusion of AMPA receptors. *Nature*, 549(7672):384–388.

Petrini, E. M., Lu, J., Cognet, L., Lounis, B., Ehlers, M. D., and Choquet, D. (2009). Endocytic trafficking and recycling maintain a pool of mobile surface AMPA receptors required for synaptic potentiation. *Neuron*, 63(1):92–105.

Plant, K., Pelkey, K. A., Bortolotto, Z. A., Morita, D., Terashima, A., McBain, C. J., Collingridge, G. L., and Isaac, J. T. R. (2006). Transient incorporation of native GluR2-lacking AMPA receptors during hippocampal long-term potentiation. *Nature Neuroscience*, 9(5):602–604.

Ranft, J., Almeida, L. G., Rodriguez, P. C., Triller, A., and Hakim, V. (2017). An aggregation-removal model for the formation and size determination of postsynaptic scaffold domains. *PLOS Computational Biology*, 13(4):e1005516.

Redondo, R. L. and Morris, R. G. M. (2010). Making memories last: the synaptic tagging and capture hypothesis. *Nature Reviews Neuroscience*, 12(1):17–30.

Sanhueza, M., Fernandez-Villalobos, G., Stein, I. S., Kasumova, G., Zhang, P., Bayer, K. U., Otmakhov, N., Hell, J. W., and Lisman, J. (2011). Role of the CaMKII/NMDA receptor complex in the maintenance of synaptic strength. *Journal of Neuroscience*, 31(25):9170–9178.

Sanhueza, M. and Lisman, J. (2013). The CaMKII/NMDAR complex as a molecular memory. *Molecular Brain*, 6(1):10.

Schnell, E., Sizemore, M., Karimzadegan, S., Chen, L., Bredt, D. S., and Nicoll, R. A. (2002). Direct interactions between PSD-95 and stargazin control synaptic AMPA receptor number. *Proceedings of the National Academy of Sciences*, 99(21):13902–13907.

Schuss, Z., Singer, A., and Holcman, D. (2007). The narrow escape problem for diffusion in cellular microdomains. *Proceedings of the National Academy of Sciences*, 104(41):16098–16103.

Sekimoto, K. and Triller, A. (2009). Compatibility between itinerant synaptic receptors and stable postsynaptic structure. *Physical Review E*, 79(3).

Sheng, M. and Hoogenraad, C. C. (2007). The postsynaptic architecture of excitatory synapses: A more quantitative view. *Annual Review of Biochemistry*, 76(1):823–847.

Shi, S.-H., Hayashi, Y., Esteban, J. A., and Malinow, R. (2001). Subunit-specific rules governing AMPA receptor trafficking to synapses in hippocampal pyramidal neurons. *Cell*, 105(3):331–343.

Shomar, A., Geyrhofer, L., Ziv, N. E., and Brenner, N. (2017). Cooperative stochastic binding and unbinding explain synaptic size dynamics and statistics. *PLOS Computational Biology*, 13(7):e1005668.

Shouval, H. Z. (2005). Clusters of interacting receptors can stabilize synaptic efficacies. *Proceedings of the National Academy of Sciences*, 102(40):14440–14445.

Tanaka, H. and Hirano, T. (2012). Visualization of subunit-specific delivery of glutamate receptors to postsynaptic membrane during hippocampal long-term potentiation. *Cell Reports*, 1(4):291–298.

Tanaka, J., Horiike, Y., Matsuzaki, M., Miyazaki, T., Ellis-Davies, G. C. R., and Kasai, H. (2008). Protein synthesis and neurotrophin-dependent structural plasticity of single dendritic spines. *Science*, 319(5870):1683–1687.

Tardin, C., Cognet, L., Bats, C., Lounis, B., and Choquet, D. (2003). Direct imaging of lateral movements of AMPA receptors inside synapses. *The EMBO Journal*, 22(18):4656–4665.

Tomita, S., Adesnik, H., Sekiguchi, M., Zhang, W., Wada, K., Howe, J. R., Nicoll, R. A., and Bredt, D. S. (2005a). Stargazin modulates AMPA receptor gating and trafficking by distinct domains. *Nature*, 435(7045):1052–1058.

Tomita, S., Stein, V., Stocker, T. J., Nicoll, R. A., and Bredt, D. S. (2005b). Bidirectional synaptic plasticity regulated by phosphorylation of stargazin-like TARPs. *Neuron*, 45(2):269–277.

Turetsky, D., Garringer, E., and Patneau, D. K. (2005). Stargazin modulates native AMPA receptor functional properties by two distinct mechanisms. *Journal of Neuroscience*, 25(32):7438–7448.

Wang, Z., Edwards, J. G., Riley, N., Provance, D. W., Karcher, R., dong Li, X., Davison, I. G., Ikebe, M., Mercer, J. A., Kauer, J. A., and Ehlers, M. D. (2008). Myosin vb mobilizes recycling endosomes and AMPA receptors for postsynaptic plasticity. *Cell*, 135(3):535–548.

Wu, D., Bacaj, T., Morishita, W., Goswami, D., Arendt, K. L., Xu, W., Chen, L., Malenka, R. C., and Südhof, T. C. (2017). Postsynaptic synaptotagmins mediate AMPA receptor exocytosis during LTP. *Nature*, 544(7650):316–321.

Yang, Y., b. Wang, X., Frerking, M., and Zhou, Q. (2008). Spine expansion and stabilization associated with long-term potentiation. *Journal of Neuroscience*, 28(22):5740–5751.

Yudowski, G. A., Puthenveedu, M. A., Leonoudakis, D., Panicker, S., Thorn, K. S., Beattie, E. C., and von Zastrow, M. (2007). Real-time imaging of discrete exocytic events mediating surface delivery of AMPA receptors. *Journal of Neuroscience*, 27(41):11112–11121.

Zamanillo, D., Sprengel, R., Hvalby, O., Jensen, V., Burnashev, N., Rozov, A., Kaiser, K. M. M., Köster, H. J., Borchardt, T., Worley, P., Lübke, J., Frotscher, M., Kelly, P. H., Sommer, B., Andersen, P., Seeburg, P. H., and Sakmann, B. (1999). Importance of AMPA receptors for hippocampal synaptic plasticity but not for spatial learning. *Science*, 284(5421):1805–1811.

Zheng, N., Jeyifous, O., Munro, C., Montgomery, J. M., and Green, W. N. (2015). Synaptic activity regulates AMPA receptor trafficking through different recycling pathways. *eLife*, 4.

Figures

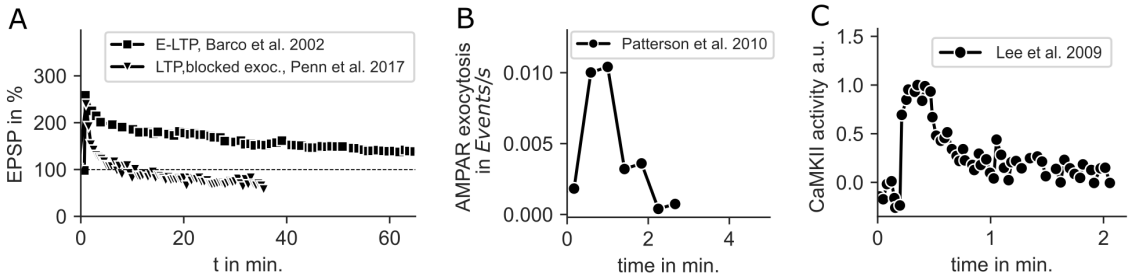

Figure 1: Temporal course of E-LTP and related processes. **(A)** E-LTP decays after 1-6 hours (squares; data taken from Barco et al., 2002) , while L-LTP remains stable for hours to days (Abraham, 2003; not depicted here). When exocytosis is blocked at the postsynaptic spine, E-LTP decays after 10-20 min (triangles; data taken from Penn et al., 2017). **(B)** The exocytosis rate is increased for a few minutes after LTP-induction (data taken from Patterson et al., 2010). **(C)** The activity of CaMKII is also increased for a few minutes after LTP-induction (data taken from Lee et al., 2009). The data has been adapted from Barco et al. (2002) Fig. 3c, Penn et al. (2017) Fig. 2c, Patterson et al. (2010) Fig. 4a, Lee et al. (2009) Fig.2b.

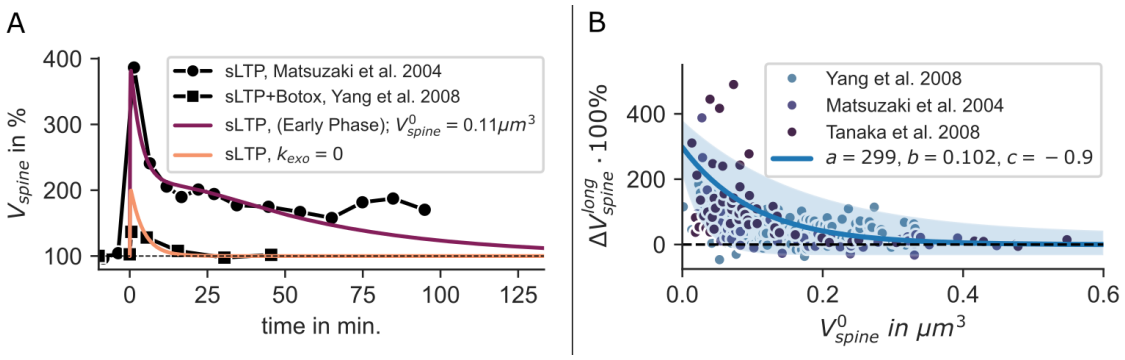

Figure 2: The enlargment of the spine during sLTP depends on exocytosis, protein synthesis and the initial spine volume V^0_{spine}. **(A)** During sLTP induction, the spine volume increases rapidly. However, in the absence of exocytosis, this increase is small and brief (squares) compared to sLTP under normal conditions (circles). Our model of sLTP (Equation 11) reproduces these experimental observations (solid lines). Note that in this study we assume that protein synthesis does not occur to model E-LTP. Therefore, in the model (purple line), the spine volume decays faster than in the experimental data, which shows sLTP under normal conditions (circles). **(B)** The initial spine volume V^0_{spine} influences the relative long-term increase in spine volume ΔV^{long}_{spine} due to sLTP (Matsuzaki et al., 2004; Tanaka et al., 2008; Yang et al., 2008), which our model accounts for via Equation 10.

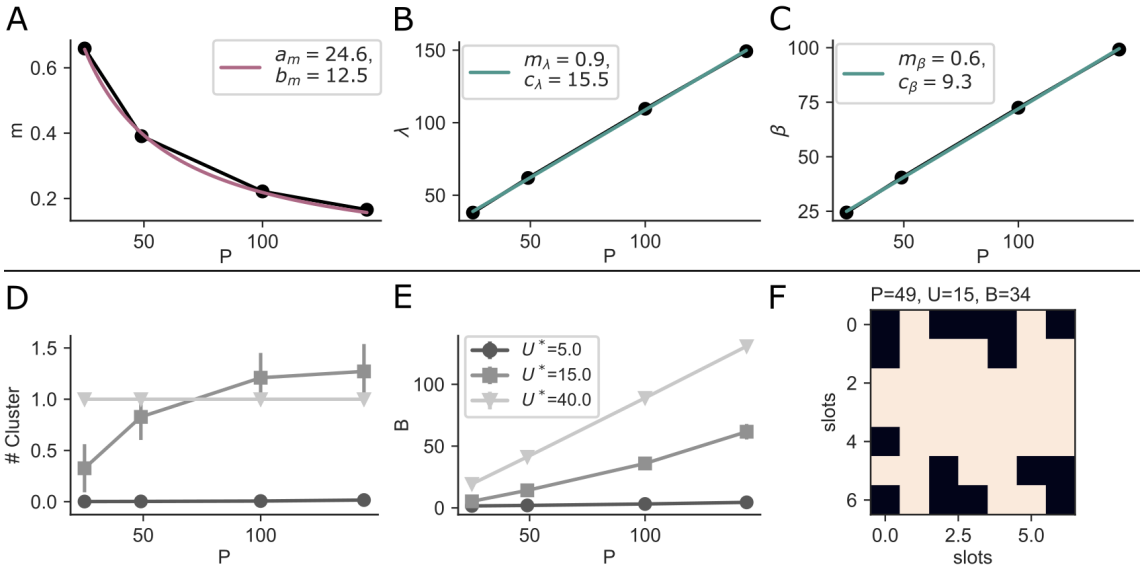

Figure 3: Functional relations in the detailed model of cooperative binding. **(A)** The slope $m(P)$ of the relation between the mean cooperative binding rate $\langle \hat{k}_{UB} \rangle$ and the number of bound receptors B depends on P, as on small grids the mean number of nearest neighbours increases faster than on large grids. **(B,C)** The mean unbinding rate $\langle \hat{k}_{BU} \rangle$ decreases with B with functions (B) $\lambda(P)$ and (C) $\beta(P)$. **(D)** The number of clusters ($>$ 5 Receptors) per PSD depends on P and the number of available mobile receptors U. **(E)** The mean number of bound receptors increases linear with P and slopes depending on U. **(F)** An example of the model with one large clusters. black: free slots; white: occupied slots

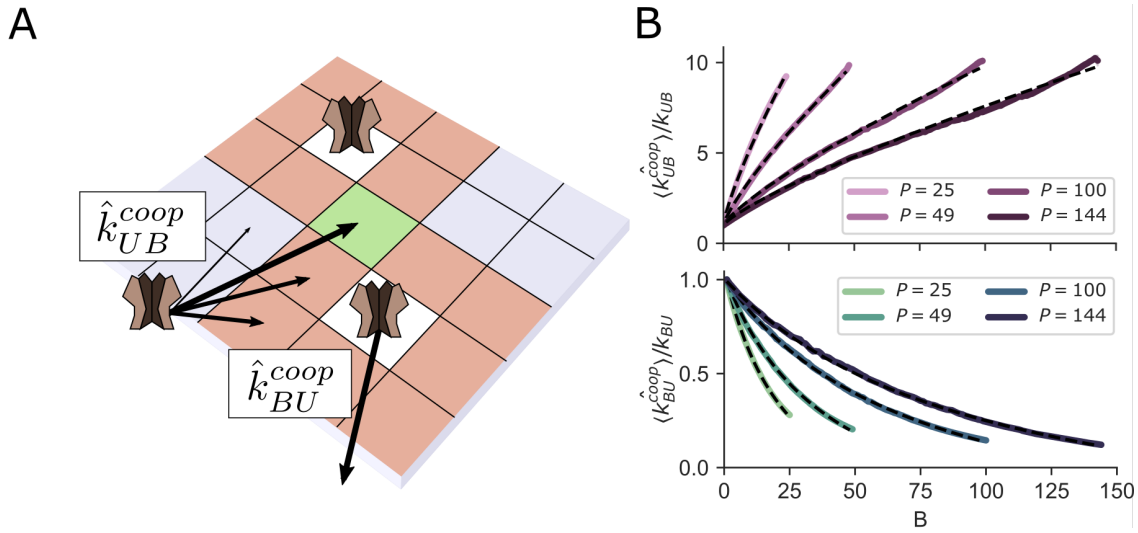

Figure 4: Basic principles and results of cooperative receptor binding. **(A)** In the cooperative binding model, the slots of the PSD are spatially ordered into a grid with each slot having a binding $\hat{k}_{UB}^{coop}$ and unbinding $\hat{k}_{BU}^{coop}$ rate dependent on the number of bound receptors being in the nearest vicinity indicated by different colors (white: low; red: intermediate; green: high). **(B)** To integrate the effects of cooperative binding into the basic model, we calculate the mean binding $\langle \hat{k}_{UB}^{coop} \rangle$ and unbinding rate $\langle \hat{k}_{BU}^{coop} \rangle$. In a stochastic simulation of the model, $\hat{k}_{UB}^{coop}$ and $\hat{k}_{BU}^{coop}$ are averaged across the grid and 10 trials in dependence of the current number of bound receptors B and for varying grid sizes (slots P). The simulation results are fitted by Equations 21 and 20 (dashed lines, for details see Materials and Methods).

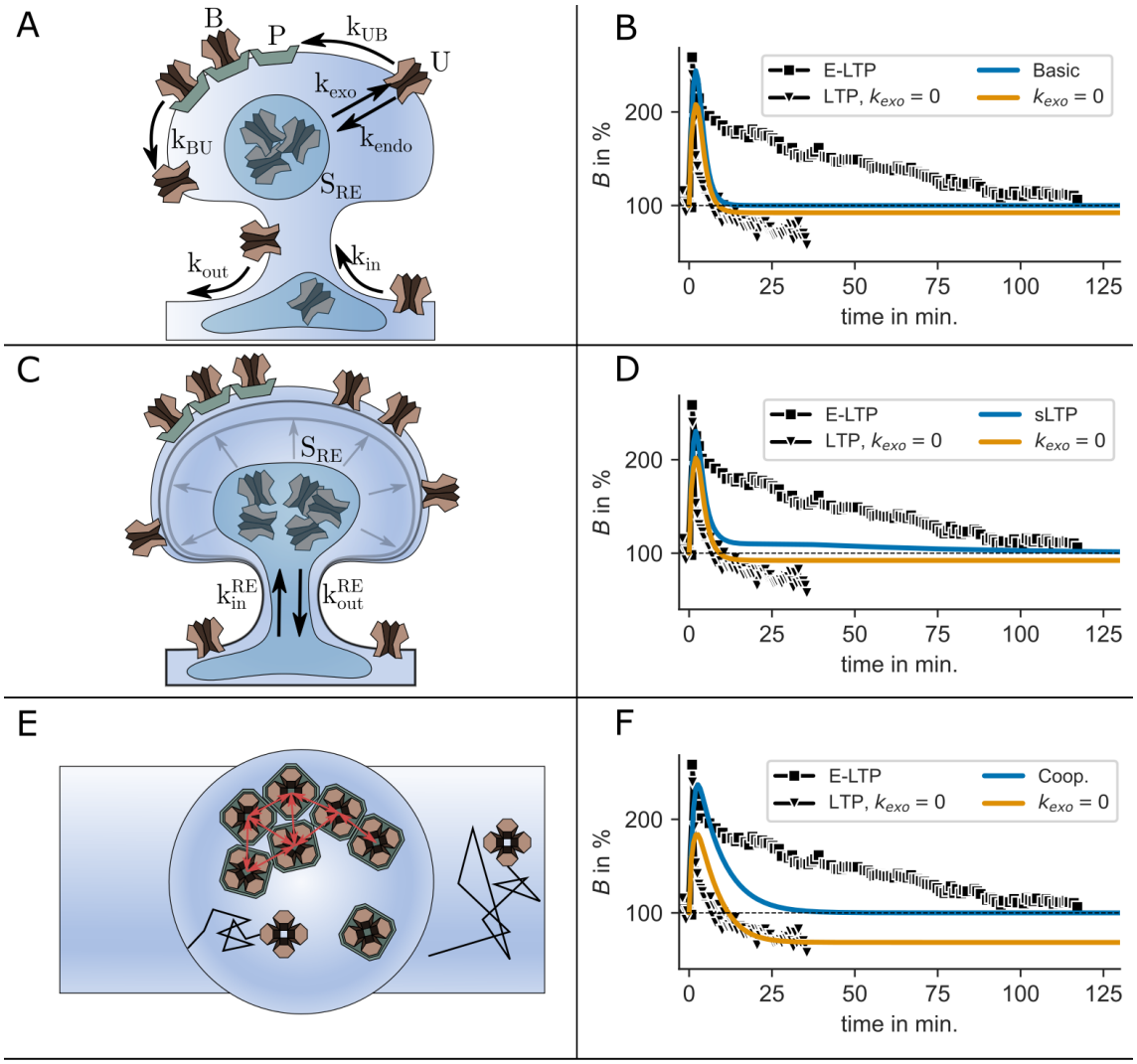

Figure 5: Different model versions and resulting AMPAR dynamics compared to experimental data. **(A)** Basic model: AMPA receptors are trafficked across the spine via several pathways. During LTP-induction exocytosis (k_{exo}) and binding rate (k_{UB}) are briefly increased. **(B)** The LTP-induced dynamics of the basic model (blue line) is compared to experimental data (black squares; Barco et al., 2002) also with the blockage of exocytosis (orange line compared to black triangles; Penn et al., 2017). **(C)** sLTP and RE trafficking model: In addition to k_{exo} and k_{UB}, we model the influence of the LTP-induced increase in spine volume and RE trafficking on AMPAR dynamics. Note that the spine volume only slowly decays back to the baseline if exocytosis occurs but rapidly decays otherwise (Figure 2; Bosch et al., 2014; Yang et al., 2008). **(D)** Similar to (B), the AMPAR-dynamics resulting from the morphological model is compared to experimental data without (blue line) and with (orange line) blockage of exocytosis.

Figure 5: **(E)** Cooperative model: In addition to the basic model, we model the influence of cooperative receptor binding on AMPAR dynamics. **(F)** Similar to (B), the AMPAR-dynamics resulting from the cooperative model is compared to experimental data without (blue line) and with (orange line) blockage of exocytosis. **(B,D,F)** LTP-induction is triggered at time point $10s$.

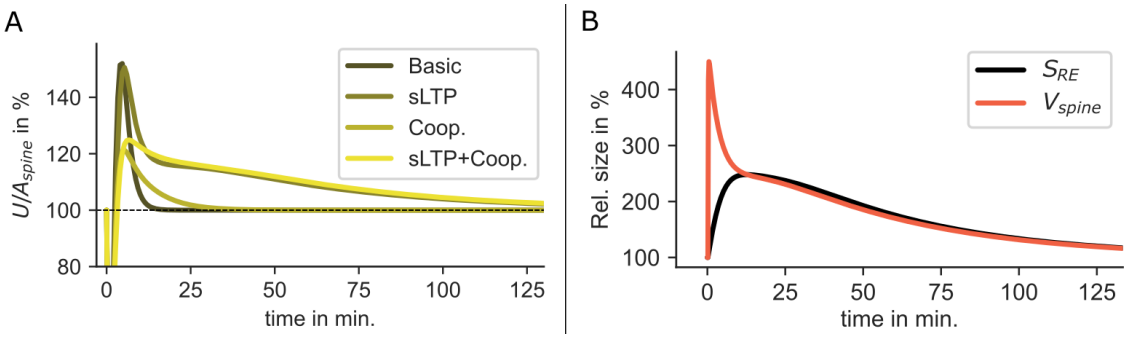

Figure 6: RE trafficking and cooperative binding influence the concentration of mobile AMPARs at the spine. **(A)** The concentration of mobile receptors U/A_{spine} increases after LTP-induction but is only sustained if accompanied by sLTP and increased trafficking of AMPARs from recycling endosomes. **(B)** The amount of recycling endosomes S_{RE} that contributes to AMPAR exocytosis (black line) and enlargement of the spine volume V_{spine} (orange line) are interdependent and increase following LTP induction (Equations 13 and 11).

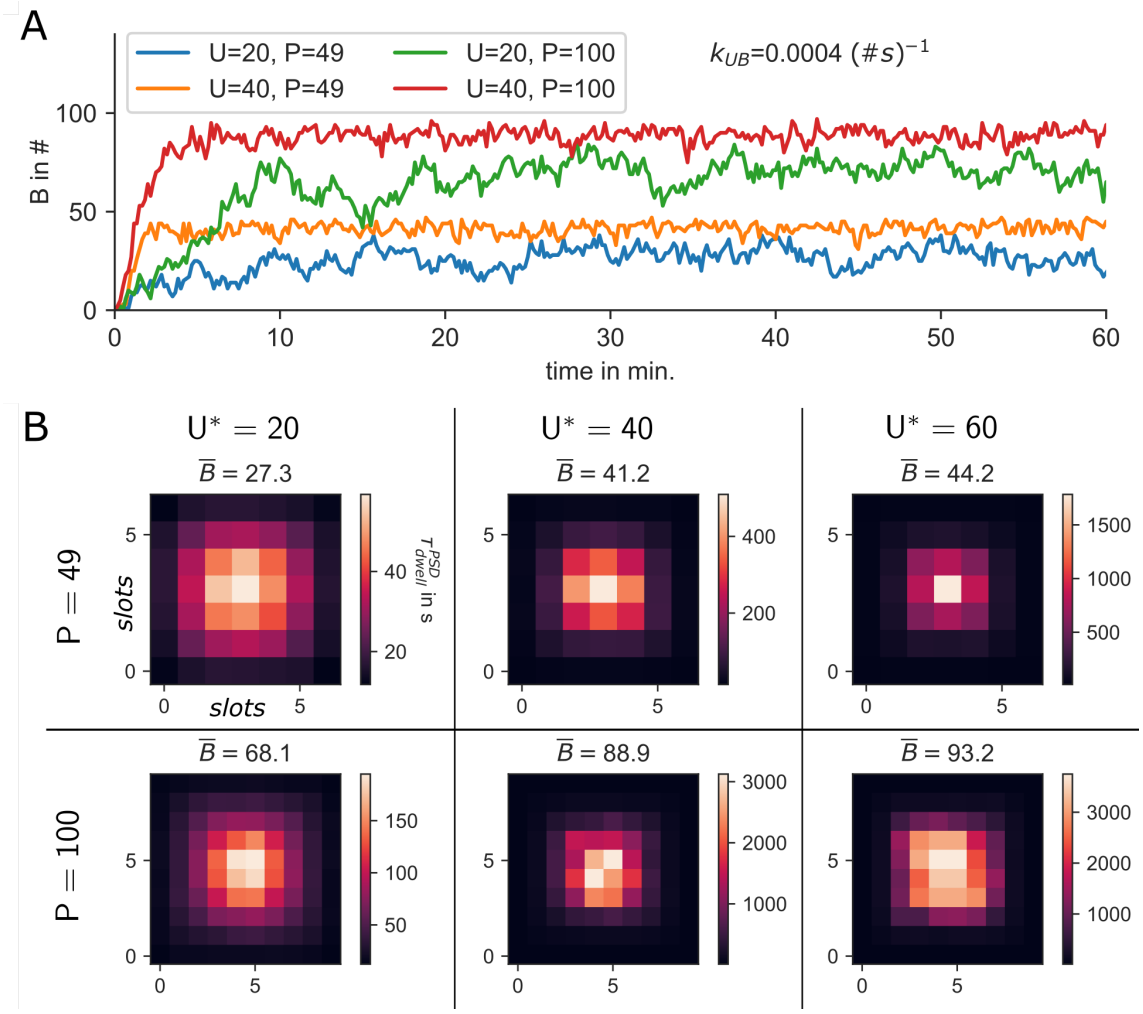

Figure 7: The clustering model used in this study shows that receptors, that lie at the core of a nanodomain/cluster, have dwell times being several orders of magnitude higher than those at the boarder. **(A)** Independent of the number of receptors or the size of the PSD, the system reaches an equilibrium in which the average number of bound receptors remains stable. The fluctuations around the average value depend on the number of available or rather mobile receptors. As shown in Shomar et al. (2017), the bound receptors form a cluster. **(B)** Receptors being at the border of such a cluster have on average a lower dwell time τ^{PSD}_{dwell} than receptors being in the core of the formed cluster. The detailed statistic of the dwell time depends on the parameters of the system such as the number of receptors or the size of the PSD. For example, a mobile pool of size $U^* = 20$ (B, top left) implies a maximal average dwell time of bound receptors at the core of the cluster of $\approx 1min.$. If the mobile pool is increased ($U^* = 40$, top middle), the maximal dwell time becomes $\approx 8min.$.

Figure 7: If the PSD size is increased, the maximal dwell times for $U^* = 40$ increases to $\approx 50min$. (bottom middle) matching the time scales observed from FRAP experiments. Please note that these results also imply a wide range of lifetimes of a cluster as measured by Nair et al. (2013).

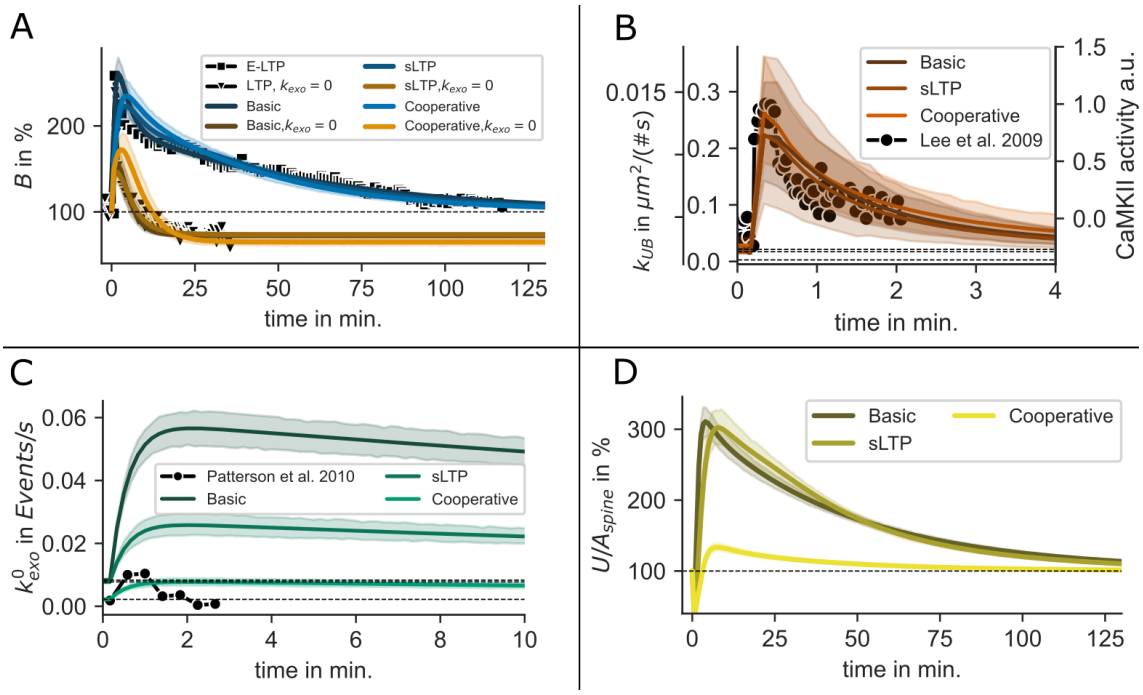

Figure 8: Variation of parameter values yields parameter sets for all three model versions such that E-LTP is maintained for several hours. **(A)** The experimentally measured temporal course of E-LTP with and without the blockage of exocytosis is matched by all three model versions (basic, sLTP, cooperative) with corresponding parameter sets. Please note that lines overlie each other. **(B,C)** For the parameter sets used in (A), the LTP-induced increase of the binding rate of the models matches experimental data of CaMKII (B) (y-axis left: rightmost for the non-cooperative models, leftmost for the cooperative), while the exocytosis rate is too high for the basic and morphological model and decays too slow for all three model versions (C). **(D)** The concentration of mobile receptors U increases to 300% of the baseline level for the basic and the morphological model but only to $\approx$ 130% for cooperative model. (A-D) Shown are the upper 1% that match best with the experimental data in (A). For the matching we used the cost function described by equation 8. Shades indicate standard deviation across parameter sets.

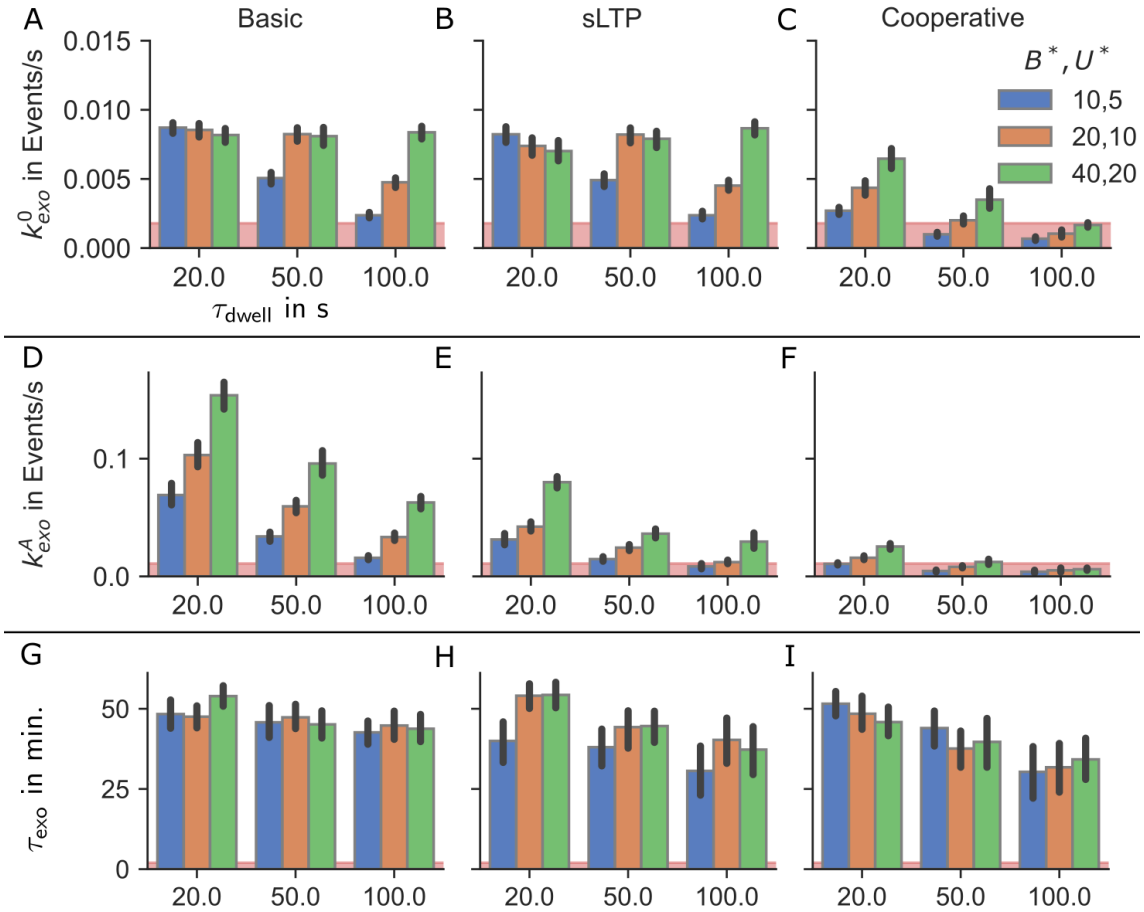

Figure 9: The parameter values of exocytosis for the best 1% parameter sets depend on the number of bound AMPARs under basal condition and the dwell time of mobile receptors at the spine. For the three models of AMPAR-dynamics (first column: basic model; second column: model with sLTP; third column: model with cooperative binding), the exocytosis rate under basal condition (k^0_{exo}; first row), the maximal amplitude of LTP-induced exocytosis rate ($k^A_{exo} = k^0_{exo}(1 + A_{exo})$; second row), and the decay of the exocytosis rate after LTP-induction (τ_{exo}; third row) are shown. Each dot corresponds to one set of parameters. The red areas indicate the biologically plausible regime of the corresponding indicators based on experimental studies (Passafaro et al., 2001; Yudowski et al., 2007; Patterson et al., 2010). Shown are the means weighted by the inverse of the cost function used in the matching procedure (Equation 8).

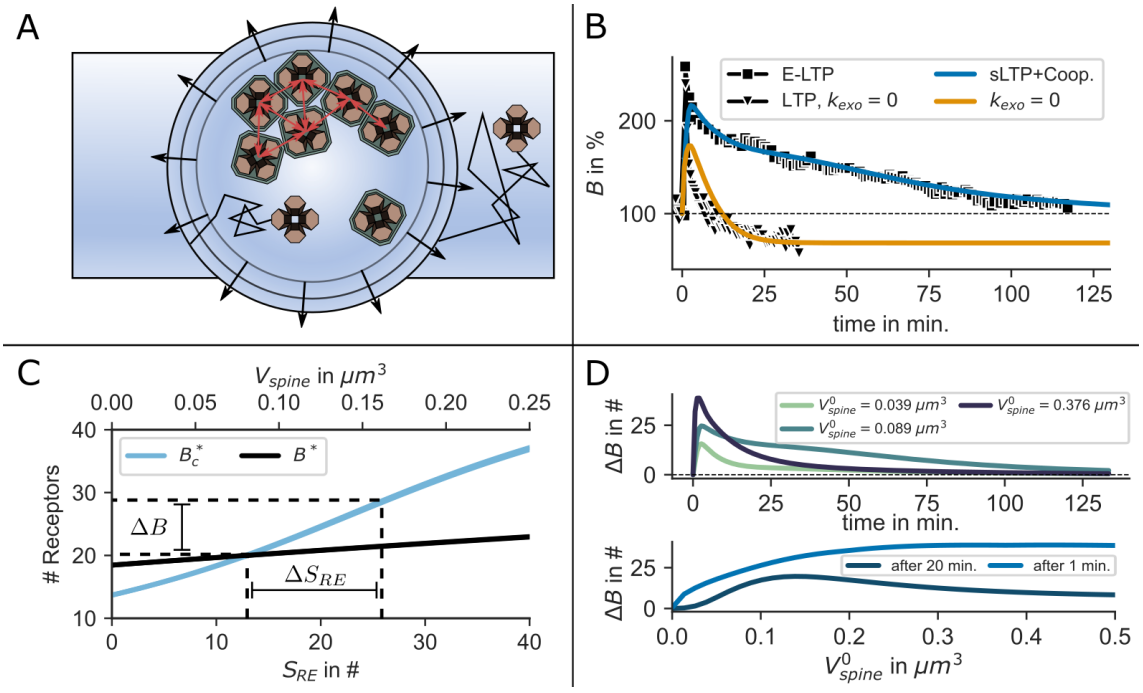

Figure 10: Cooperative binding and morphological changes complement each other to sustain E-LTP. **(A)** Combined model: Cooperative binding enables AMPARs to form clusters in the PSD and morphological changes of the spine head accompanied by RE mobilization towards the spine modulate the trafficking of receptors. **(B)** Similar to Figure 5, the LTP-induced dynamics of the combined model with experimentally derived parameters (blue line) is compared to experimental data (black squares; Barco et al., 2002) also with the blockage of exocytosis (orange line compared to black triangles; Penn et al., 2017). **(C)** The dependency of the number of bound AMPARs in the PSD (fixed point B^*) on the volume of the spine head (V_{spine}) and the amount of exocytosis from REs (S_{RE}) respectively with cooperative binding (blue line, B_c^*) compared to systems without cooperative binding (black line, B^*). **(D)** The maintenance of E-LTP depends on the spine volume before LTP-induction V^0_{spine}. Top: the temporal development of E-LTP for three different spine volumes. Bottom: the level of E-LTP at two different points in time (blue: $1min$ after LTP-induction; dark blue: $20min$ after LTP-induction) for a wide range of initial spines volumes. Here, the PSD size P depends on the initial spine head volume. In **B,C**, as for Figure 5D, the initial spine volume is $V^0_{spine} = 0.08\mu m^3$ and the number of slots $P = 70$.

Tables

Table 1: Parameters of AMPAR trafficking.

Parameter	Meaning	Value	Experiments
k^0_{exo}	Rate of exocytosis of new receptors under basal condition	0.0018 s^-1	Patterson et al. (2010)
k_{endo}	Rate of receptor endocytosis in the spine	0.0021 $\mu m^2/s$	this study (Equation 3)
τ_{dwell} $(1/k_{out^0})$	Dwell time of mobile receptors in the spine	50 s	Ehlers et al. (2007); Borgdorff and Choquet (2002), this study
k_{in}	Rate at which AMPARs enter the spine via lateral diffusion	0.2 $\#/s$	Ashby et al. (2006); Frischknecht et al. (2009); Makino and Malinow (2009); Patterson et al. (2010)
k_{BU}	Unbinding rate of receptors from PSD slots	0.1 s^{-1}	Heine et al. (2008)
k^0_{UB}	Binding rate of AMPARs at the PSD	0.0036 $\mu m^2/(\#s)$	this study (Equation 4)
k^0_{UB} (Coop.)	Binding rate of AMPARs at the PSD in the cooperative binding model	0.0005 $\mu m^2/(\#s)$	this study (Equation 26)
U^*, B^*	Steady state number of mobile and bound receptors at the average spine	$10, 20$	Nusser et al. (1998); Sheng and Hoogenraad (2007)
P	Number of slots at the PSD	70	this study
V_{spine}	Spine volume	$0.08\mu m^3$	Matsuzaki et al. (2004); Adrian et al. (2017)
S_{RE}	size of an AMPAR exocytosis event	13	Yudowski et al. (2007)

Table 2: Parameters of LTP-induced changes in exocytosis and binding rate.

Parameter	Meaning	Value	Experiments
A_{UB}	Factor of LTP-induced increase in binding rate in the basic model	30	this study
A_{UB} $(Coop.)$	Factor of LTP-induced increase in binding rate in the cooperative binding model	5	this study
$\tau_{UB}^{increase}$	Time constant of increase of binding rate	$5s$	Lee et al. (2009)
τ_{UB}	Time constant of decay of binding rate	$60s$	Lee et al. (2009)
A_{exo}	Factor of LTP-induction increase in exocytosis	5	Patterson et al. (2010); Kennedy et al. (2010)
$\tau_{exo}^{increase}$	Time constant of increase of exocytosis rate	$25s$	Patterson et al. (2010)
τ_{exo}	Time constant of decrease of exocytosis rate	$60s$	Patterson et al. (2010)

Table 3: Parameter range for the Monte-Carlo method.

Parameter	Meaning	Range
k_{exo}^{0}	Rate of exocytosis of new receptors into the spine membrane under basal conditions.	$0...0.1\#/s$
τ_{exo}	Time constant with which the exocytosis rate decreases back to its baseline after LTP-induction.	$0...67min.$
A_{exo}	Factor by which the exocytosis rate increases upon LTP-induction.	0...20
k_{BU}	Unbinding rate of AMPARs from slots at the PSD.	$0...1s^{-1}$
τ_{UB}	Time constant with which the binding rate decreases back to its baseline after LTP-induction.	$0...8min.$
A_{UB}	Factor by which the binding rate increases upon LTP-induction.	0...50
$A_{UB}(Coop.)$	Factor by which the binding rate increases upon LTP-induction in the cooperative binding model.	0...10

Table 4: Parameter values from fitting EPSP data taken from Penn et al. (2017) (LTP with blocked exocytosis) and Barco et al. (2002) (E-LTP)

Parameter	Meaning	Value	
		x: E-LTP	x: $k_{exo} = 0$
$T_{x,short}$	decay time constant	$82s$	$42s$
$T_{x,long}$	decay time constant	$3445s$	$605s$
$T^{increase}_{x,short}$	rise time constant	$1s$	$18s$
$T^{increase}_{x,long}$	rise time constant	$128s$	$42s$
$C_{x,short}$	baseline amplitude	98%	84%
$C_{x,long}$	baseline amplitude	-2%	-16%
$A_{x,short}$	increase in amplitude during LTP	253%	185%
$A_{x,long}$	increase in amplitude during LTP	97%	57%